Title

Development of Methods for Analyzing Tibiofemoral Kinematics and Contact Kinematics using 3D Models

Author

Simileysky, Alexander

Publication Date

2021

Peer reviewed|Thesis/dissertation

Development of Methods for Analyzing Tibiofemoral Kinematics and Contact Kinematics using 3D Models

By

ALEXANDER SIMILEYSKY
THESIS

Submitted in partial satisfaction of the requirements for the degree of

MASTER OF SCIENCE

in

Biomedical Engineering

in the

OFFICE OF GRADUATE STUDIES

of the

UNIVERSITY OF CALIFORNIA

DAVIS

Approved:

Maury L. Hull, Chair

Susan Stover

Gavin C. Pereira

Committee in Charge

2021

ABSTRACT

Background: Tibiofemoral kinematics describe the relative movement of the femur with respect to the tibia through flexion, which provides an objective assessment of joint function and can be used to determine whether an artificial knee restores natural movement following total knee arthroplasty (TKA). One way to measure tibiofemoral kinematics is by analyzing the anterior-posterior (AP) movement of the femoral condyles on the tibia. There are two common methods for identifying AP positions and hence condylar movements: 1) the flexion facet center (FFC), and 2) the lowest point (LP) methods. However, comparison of AP positions from the two methods in the native knee yielded contradictory findings.

Three factors need to be considered before applying the FFC and LP methods. The first factor is the selected reference plane upon which the AP positions are measured. One useful plane is the plane perpendicular to the tibial mechanical axis, which allows the AP positions to be expressed in a direction consistent with the coordinate system of Grood and Suntay. However, to construct a reliable tibial mechanical axis and hence perpendicular plane, there is a need for a highly repeatable and reproducible method for identifying the distal point of the tibial mechanical axis (i.e. center of the talocrural joint). A second factor is the presence of cartilage on the 3D model of the femur, which may alter the shape of the femoral articular surface and hence positions of the FFCs and LPs. A third factor is the smoothness of the 3D model, which may also alter the shape of the femoral articular surface.

Hence the objective of Chapter 1 was to determine the repeatability and reproducibility of a new method and two previously described methods for locating the center of the talocrural joint. After constructing the tibial mechanical axis using the most repeatable and reproducible method from Chapter 1, the objectives of Chapter 2 were to use the plane perpendicular to the

tibial mechanical axis to determine how well the FFC and LP methods agree, and to determine whether the addition of articular cartilage and/or smoothing significantly affects the AP positions of the femoral condyles.

Another subject of interest is tibiofemoral contact kinematics, which describe the movement of locations of contact by the femur on the tibia throughout flexion. Knowledge of the AP tibial contact locations in artificial knees is useful in assessing wear of tibial inserts and detecting posterior rim loading. However, existing methods for determining AP tibial contact locations based on analysis of images from single-plane fluoroscopy, such as the penetration method, are prone to error. Hence, the objectives of Chapter 3 were to create a new planar model that can determine AP tibial contact locations and determine whether errors of the planar model are lower than those of the penetration method.

Methods: For Chapter 1, the medial-lateral (ML), AP, and proximal-distal (PD) coordinates of the center of the talocrural joint were determined in thirteen 3D bone models of the full tibia using the new method, termed the area centroid method, and the previously described diagonal intersection and biplanar methods. Intraobserver and interobserver intraclass correlation coefficients (ICCs) were computed to quantify the repeatability and reproducibility for each method.

For Chapter 2, Magnetic Resonance (MR) images of the native knee were obtained from eleven subjects, who subsequently performed a deep knee bend under fluoroscopy. For each subject, four different MR models of the distal femur were created: femur bone, smoothed femur bone, femur bone with cartilage, and femur bone with smoothed cartilage. AP positions of the LPs and FFCs in each compartment were determined for each model type following 3D model-to-2D image registration.

For Chapter 3, a slopes-of-sagittal profiles (SSP) model was created using mathematical functions to simulate articular surfaces of the tibial insert and femoral condyles. AP tibial contact locations were calculated using the model and the penetration method and simultaneously measured with a tibial force sensor in 10 cadaveric TKA knees for four flexion angles (0°, 30°, 60°, and 90°) in each compartment during passive motion. For each method, the overall bias, overall precision, and overall root mean square error (RMSE) were calculated from the differences between the computed AP tibial contact locations and the measured locations.

Results: For Chapter 1, the area centroid method had excellent repeatability (ICC ≥ 0.97) and reproducibility (ICC ≥ 0.92). For the biplanar method, repeatability (ICC ≥ 0.86) was good and reproducibility (ICC ≥ 0.40) was fair. For the diagonal intersection method, repeatability (ICC ≥ 0.71) was moderate and reproducibility (ICC ≥ 0.46) was fair.

For Chapter 2, the limits of agreement were ± 5.5 mm at 0° flexion, and bounded by ± 2.4 mm at 30°, 60°, and 90° flexion. The differences in AP positions between the four model types were minimal for both LPs and FFCs.

For Chapter 3, the SSP model had an overall bias of 0.6 mm and precision of 2.8 mm which were significantly greater than the overall bias of -0.1 mm ($p = 0.0369$) and overall precision of 2.0 mm ($p = 0.0021$) of the penetration method.

Conclusion: The area centroid method offered better repeatability and reproducibility than existing methods and is recommended when identifying the mechanical axis of the tibia. Meanwhile, the FFC and LP methods provided similar mean results during a deep knee bend at flexion angles of 30° and beyond but not at 0°. The lack of significant differences between model types in the AP positions of the femoral condyles indicate that addition of cartilage to 3D bone models is not required to accurately determine AP positions. Therefore, faster and less expensive

imaging techniques such as CT can be used confidently to acquire the 3D bone models for the analysis of tibiofemoral kinematics. Finally, a planar model based on the analysis of single-plane radiographic images did not increase accuracy in AP tibial contact locations. Hence, the penetration method is preferred to determine AP tibial contact locations using single-plane radiography.

PREFACE

This research is presented in the form of three independent chapters with the intention that each be suitable for submission and publication in a peer-reviewed scientific journal. As a result, there is some redundancy between the three chapters. Chapter 1 investigates the repeatability and reproducibility of a new method and two previously described methods for locating the center of the talocrural joint. Using the best method from Chapter 1, a tibial mechanical axis is constructed from which a perpendicular reference plane is defined. Chapter 2 uses the plane perpendicular to the tibial mechanical axis to investigate how well two methods for finding the AP positions of femoral condyles agree, and whether the addition of articular cartilage and/or smoothing significantly affects the AP positions. Chapter 3 investigates whether a planar model can be used to accurately determine the AP tibial contact locations.

TABLE OF CONTENTS

Chapter 1: Repeatability, Reproducibility, and Agreement of Three methods for Finding the Mechanical Axis of the Human Tibia

ABSTRACT

Background: Identifying the center of the talocrural joint is a crucial step in defining the tibia's mechanical axis, which is used in a variety of applications such as a reference for measuring alignment variables following TKA. The objectives of this study were to 1) describe a new method for determining the center of the talocrural joint, 2) determine the repeatability and reproducibility of the new method and two previously described methods for locating the center of the talocrural joint, 3) determine the limits of agreement between pairs of methods, and 4) determine angular differences in the coronal and sagittal planes between tibial mechanical axes.

Methods: Termed the area centroid method, the new method identified the center of the talocrural joint as the centroid of the distal articular surface of the tibia. Previously described methods included the diagonal intersection (Yoshioka et al., 1989) and biplanar (Marchant et al., 2005) methods. For each method, the medial-lateral (ML), anterior-posterior (AP), and proximal-distal (PD) coordinates of the center of the talocrural joint were determined in thirteen 3D bone models of the full tibia.

Results: For the area centroid method, both repeatability (ICC $\geq$ 0.97) and reproducibility (ICC $\geq$ 0.92) were excellent. For the biplanar method, repeatability (ICC $\geq$ 0.86) was good and reproducibility (ICC $\geq$ 0.40) was fair. For the diagonal intersection method, repeatability (ICC $\geq$ 0.71) was moderate and reproducibility (ICC $\geq$ 0.46) was fair. Limits of agreement of $\pm$ 4.1 mm were tightest between the area centroid and diagonal intersection methods. Angular differences between tibial mechanical axes were limited to 3º.

Conclusion: The area centroid method locates the anatomic center of the talocrural joint and offers better repeatability and reproducibility than existing methods. The area centroid method is recommended when identifying the mechanical axis of the tibia.

INTRODUCTION

The mechanical axis of the tibia is a useful reference in a variety of applications. For example, in simulations of mechanically aligned total knee arthroplasty (TKA), the proximal segment of the tibia is resected perpendicular to its mechanical axis (Gu et al., 2014). Additionally, important alignment variables such as the hip-knee-ankle angle and posterior tibial slope are measured with respect to the mechanical axis of the tibia (Yoo et al., 2008; Cherian et al., 2014). Accurate measurements of these alignment variables can help reduce TKA implant wear, prevent TKA implant loosening, and improve functional performance of the knee post-operation (Marchant et al., 2005; Yoo et al., 2008). Furthermore, there is a need for a plane that serves for tracking anterior-posterior (AP) translations and internal-external (IE) rotations of the native and prosthetic femoral condyles with respect to the tibia (Pinskerova et al., 2004; Nicolet-Petersen et al., 2019) and a useful plane is perpendicular to the mechanical axis. Finally, the mechanical axis can serve as an anatomical reference for locating the functional internal-external rotation axis (Grood & Suntay, 1983; Culvenor et al., 2016).

Defining the tibial mechanical axis involves identifying two points on the tibia, one on the proximal end representing the center of the tibiofemoral joint and one on the distal end representing the center of the talocrural joint. The proximal point for the mechanical axis is well established within the literature and is defined as the midpoint between the peaks of the intercondylar eminences (Yoshioka et al., 1989; Subburaj et al., 2009; Gu et al., 2014). However, there are disagreements regarding the method for finding the distal point representing the center of the talocrural joint. One approach is the diagonal intersection method, which defines the center of the talocrural joint as the intersection of two diagonal lines drawn from the four corners of the weight-bearing areas of the distal articular surface in the axial plane (Yoshioka et al.,

1989). Another approach is the biplanar method, where the center of the talocrural joint is defined by the AP and proximal-distal (PD) positions of the most proximal point of the talar dome in the sagittal plane and the medial-lateral (ML) position of the midpoint of the talar dome in the coronal plane (Marchant et al., 2005). Yet a third approach new to this study is the area centroid method, which defines the center of the talocrural joint as the centroid of the weight-bearing area in an axial projection.

The objectives of this study were to 1) describe a new method for determining the distal point representing the center of the talocrural joint, 2) determine the repeatability and reproducibility of three methods for locating the center of the talocrural joint on full 3D tibia models, 3) determine the agreement between pairs of methods, and 4) determine the angular differences in the coronal and sagittal planes between pairs of tibial mechanical axes.

METHODS

Thirteen 3D bone models of native contralateral tibias from TKA patients were created from thin contiguous slice (1.25 mm (0.05 in)) computed tomography (CT) images obtained from post-operative CT scanograms. The patients were selected from a group of subjects, all of whom had no skeletal abnormalities or prior surgery in the native contralateral limb (Nicolet-Petersen et al. 2019). CT images were obtained following the Perth Protocol, and the bone models were constructed using open-source software (3D Slicer version 4.10.0). The PD direction was defined for each bone model by drawing a line through the centroids of two tibia shaft cross-sections (Figure 1.1A). AP and ML directions were defined by fitting a bounding box to the tibial plateau (Figure 1.1B). After orientation, the bone model was converted into a point cloud. The origin of the tibial coordinate system was set along the PD axis, such that the most

inferior point on the medial malleolus was coplanar with the origin in the axial plane which was perpendicular to the PD axis.

All methods for finding the center of the talocrural joint were executed using a MATLAB program. Each method started out by loading the full tibia point cloud into the program, then isolating all points that were within 50 mm above the most inferior point on the medial malleolus. The isolated points were plotted in the coronal view, and the points on the medial and lateral edges of the weight-bearing distal articular surface were selected (Figure 1.2). The medial edge was found at the start of the flat section where the medial malleolus ended, and the lateral edge was found at the end of the flat section where the bone began to curve upward. The coronal center point was computed as the midpoint between the two selected points in the coronal plane and used as a reference for determining which cross-sections would be isolated in the next steps.

The diagonal intersection method started by isolating tibia points that were within 1 mm below and within 6 mm above the coronal center point along the PD axis. Next, points belonging to the weight-bearing area of the tibia were obtained from the isolated points using a lasso selection program (D'Errico, 2007) (Figure 1.3A). The contour of the weight-bearing area points was traced in the axial plane using boundary-extraction code (Awrangjeb, 2016). Along the contour, four points were selected that best represented the corners of the weight-bearing area of the distal articular surface (Figure 1.3B). The AP and ML coordinates of the center of the talocrural joint were defined as the intersection of two diagonals drawn from the four corner points in the axial plane. The PD coordinate of the center of the talocrural joint was defined as the PD coordinate of the coronal center point.

The biplanar method, which originally relied on points on the talus, was adapted for implementation on a full 3D tibia model by using points on the distal articular surface of the tibia

corresponding to points on the proximal articular surface of the talus (Marchant et al., 2005). Still using the points isolated within 50 mm above the most inferior point on the medial malleolus, the biplanar method also isolated tibia points that were within 1 mm of a line parallel to the AP axis and passing through the coronal center point. Points within 1 mm were isolated to provide a sagittal slice with a sufficient number of points to locate the peak of the distal articular surface. The isolated points were plotted in the sagittal view and the peak of the distal articular surface was located, which defined the AP and PD coordinates of the center of the talocrural joint (Figure 1.4). The ML coordinate of the center of the talocrural joint was defined as the ML coordinate of the coronal center point.

The area centroid method is a variation of the diagonal intersection method. The weight-bearing area and contour were obtained following the same procedure as in the diagonal intersection method. The AP and ML coordinates of the center of the talocrural joint were defined as the centroid of the weight-bearing area (Figure 3C). The PD coordinate of the coronal center point was defined as the PD coordinate of the coronal center point, just like in the diagonal intersection method.

Data Analyses

Three observers determined the center of the talocrural joint using each of the three methods on five full 3D tibia models repeated five times for each method in five analysis sessions with at least 48 hours between each session (Lozano et al., 2019). The repeatability and reproducibility of the methods were determined by calculating the intraobserver and interobserver intraclass correlation coefficients (ICCs) using two-factor repeated measures analysis of variance (ANOVA) with random effects (Bartlett et al., 2008). The first factor had three levels (observers 1 to 3), and the second factor had five levels (3D tibia models 1 to 5).

Three ANOVA models were performed, one for each of the three coordinates (ML, AP, PD) for the location of the center of the talocrural joint. ICC values > 0.9 indicate excellent agreement, 0.75 – 0.90 indicate good agreement, 0.5 – 0.75 indicate moderate agreement, and 0.25 – 0.5 indicate fair agreement (Indrayan 2013).

Agreement between pairs of methods was quantified by constructing Bland-Altman plots and determining limits of agreement (Martin Bland & Altman, 1986). The plots were constructed by calculating the mean of the two methods as the independent variable and the difference between these methods as the dependent variable for each of the thirteen 3D tibia models. Angular differences between tibial mechanical axes were determined by first connecting the center points of the talocrural joint determined by each method with the midpoint between the tibial eminences. For each pair of tibial mechanical axes (e.g. area centroid and diagonal intersection), angular differences were computed in the coronal and sagittal planes. In the coronal plane, a positive angular difference indicated that the distal point of the second mechanical axis was more lateral than that of the first mechanical axis in each pair. In the sagittal plane, a positive angular difference indicated that the distal point of the second mechanical axis was more posterior than that of the first mechanical axis in each pair.

RESULTS

The intraobserver and interobserver ICC values were greatest for the area centroid method and lowest for the diagonal intersection method (Table 1.1). For repeatability (i.e. intraobserver), ICC values for the ML (0.98) and AP (0.97) coordinates of the area centroid method indicated excellent agreement and were consistently greater than those of the diagonal intersection (ML 0.71; AP 0.91) and biplanar methods (ML 0.96; AP 0.86) (Table 1.1). For reproducibility (i.e. interobserver), larger differences in ICC values between the area centroid

method and the other two methods were evident. Again, ICC values of the area centroid method indicated excellent agreement (ML 0.92; AP 0.94). For the diagonal intersection method, ICC values for the ML (0.46) and AP (0.56) coordinates indicated fair and moderate agreement, respectively, while ICC values for the ML (0.77) and AP (0.40) coordinates of the biplanar method indicated good and fair agreement, respectively.

For the Bland-Altman plots (Figure 1.5), the limits of agreement were tightest between the diagonal intersection and area centroid methods. The limits of agreement for the ML coordinate were the widest at +4.9 mm and –3.2 mm and the limits of agreement for the AP coordinate were slightly tighter at +5.5 mm and 0.0 mm. For the PD coordinate, the diagonal intersection and area centroid methods were in full agreement.

Angular differences were greatest between the diagonal intersection and biplanar methods. For the diagonal intersection and biplanar methods, the maximum absolute angular difference was 1.5° (mean: -0.2° ± 0.5°) in the coronal plane and 2.9° (mean: -1.2° ± 0.6°) in the sagittal plane. For the area centroid and diagonal intersection methods, the maximum absolute angular difference was 0.6° (mean: -0.2° ± 0.2°) in the coronal plane and 0.7° (mean: 0.4° ± 0.2°) in the sagittal plane. For the area centroid and biplanar methods, the maximum absolute angular difference was 1.1° (mean: -0.2° ± 0.5°) in the coronal plane and 2.2° (mean: -0.8° ± 0.6°) in the sagittal plane.

DISCUSSION

The objectives of this study were to describe a new method termed the ‘area centroid’ method for determining the distal point representing the center of the talocrural joint, determine the repeatability and reproducibility of the area centroid, the diagonal intersection, and the biplanar methods, determine the agreement between pairs of methods, and determine angular

differences in the coronal and sagittal planes between pairs of tibial mechanical axes. Based on the highest ICC values, one key finding was that the repeatability and reproducibility were best for the area centroid method. A second key finding was that the limits of agreement were tightest between the area centroid and diagonal intersection methods. A final key finding was that angular differences in the coronal and sagittal planes were bounded by 1.1º and 2.2º, respectively, between the area centroid and biplanar methods.

The present study has shown that the area centroid method was the most repeatable and reproducible approach to identify the center of the talocrural joint and, therefore, the distal point of the tibial mechanical axis. The high ICC values for the area centroid method can be attributed to the method's minimal user input, only requiring the points on the medial and lateral edges of the weight-bearing distal articular surface to be selected. As a result, the variability between repeated measures and observers was minimized. In addition, the area centroid method directly used the shape of the weight-bearing area to calculate the centroid, resulting in an anatomically accurate location of the center of the talocrural joint (Figure 1.3C). Moving forward, the area centroid method is recommended when identifying the mechanical axis of the tibia.

Due to its tight agreement with the area centroid method, the diagonal intersection method was the next best approach for finding the center of the talocrural joint. This tight agreement can be understood by noting that both methods isolated the same weight-bearing area to identify the center of the talocrural joint. One drawback of the diagonal intersection method was its low reproducibility, which can be attributed to the variability introduced by having to manually select four corners of the weight-bearing area. Although there was a standardized guide for choosing the four corner points, the location of each individual corner remained subjective, especially along the lateral edge of the weight-bearing area.

The poor agreement between the area centroid and biplanar methods can be attributed to the ML position of the sagittal slice. In the biplanar method, the ML position of the sagittal slice and the ML coordinate for the center of the talocrural joint were defined using the ML coordinate of the coronal center point, which could vary based on the chosen points for medial and lateral edges of the distal articular surface. Consequently, the limits of agreement for the ML coordinates widened. Furthermore, the variability in the ML position of the sagittal slice propagated to the AP position for the peak of the distal articular surface in that sagittal slice, which defined the AP coordinate for the center of the talocrural joint. Thus, the limits of agreement for the AP coordinate also widened.

Although angular differences between methods were relatively small, nevertheless differences are clinically important for certain applications. Greater differences occurred between the area centroid and biplanar methods than between the area centroid and diagonal intersection methods. A 1º difference in the coronal plane would be clinically important when determining the hip-knee-ankle angle, which is measured between the mechanical axes of the femur and tibia (Cherian et al., 2014). Likewise, a 2º difference in the sagittal plane would be clinically important when determining the posterior tibial slope, which is measured with reference to the tibial mechanical axis (Yoo et al., 2008).

Although angular differences between the area centroid method and diagonal intersection methods were limited to less than 1°, repeatability and reproducibility are important metrics in assessing the quality of a method. Thus, the most desirable method for finding the center of the talocrural joint is one that produces the most repeatable and reproducible results providing that the complexity of implementing the method is not markedly increased over existing methods.

The area centroid method was the most repeatable and reproducible and was implemented without increased complexity.

One methodological issue which merits discussion is the definition of the mechanical axis used in this study. In the literature, the mechanical axis of the tibia was defined as a straight line connecting the center of the knee joint and the center of the talocrural joint (Luo, 2004; Yoo et al., 2008; Subburaj et al., 2009; Cherian et al., 2014). For this study, the center of the talocrural joint was defined as the anatomical center of the distal articular surface of the tibia, which was consistent with the literature (Yoshioka et al., 1989; Yoo et al., 2008; Subburaj et al., 2009). Another way the center of the talocrural joint could have been defined is as the functional center of the talocrural joint, which does not rely on anatomical references (Siston et al., 2005). However, the latter method is disadvantageous because of the complexity in finding the functional center using motion tracking devices and poor repeatability. Accordingly, a new anatomical method was developed in the present study and compared to existing anatomical methods.

Another methodological issue is that the study focused on methods for finding the center of the talocrural joint that were restricted to a 3D model of the tibia per se. A common anatomic method defines the center of the talocrural joint as the midpoint of a line connecting the medial and lateral malleoli (Marchant et al., 2005; Siston et al., 2005; Subburaj et al., 2009). Because the lateral malleolus is a feature of the fibula, this method cannot be performed with a 3D model of the tibia sans fibula. Regardless, malleoli methods had large errors indicative of poor repeatability in the estimation of the AP and ML coordinates for the center of the talocrural joint (Siston et al., 2005) so that their inclusion is not expected to affect the conclusion of our study

that the area centroid method is recommended based on superior repeatability and reproducibility.

A potential limitation of our study concerns the number of tibias included. Although 13 tibias may not represent the variation in anatomy of the population, nevertheless the number was sufficient for the purposes of our study. Computing ICC values relied on a subset of this number and 13 tibias was sufficient to generate Bland and Altman plots, which showed wide variation in agreement between pairs of methods. In the analysis of angular differences, differences were detected between the methods which are clinically relevant. Accordingly, increasing the sample size would not change the key results of our study.

CONCLUSION

This study developed the area centroid method, which is a new method, for finding the center of the talocrural joint using 3D tibia models and showed that this method is superior to two existing methods. The superiority lies in using the shape of the weight-bearing area to calculate the centroid, resulting in an anatomically accurate location of the center of the talocrural joint, and in high ICC values. Hence the area centroid method is recommended when identifying the mechanical axis of the tibia.

ACKNOWLEDGMENT

The authors are grateful to Medacta USA, Inc. for financial support. We also thank William Bradford, Ethan Rego, and Dana Carriger for assisting with the ICC analysis.

REFERENCES

Awrangheb, M., 2016. Boundary extraction (identification and tracing) from point cloud data, 1.0 ed, MATLAB Central File Exchange.

Bartlett, J.W., Frost, C., 2008. Reliability, repeatability and reproducibility: Analysis of measurement errors in continuous variables. Ultrasound Obstet. Gynecol. 31, 466-475.

Cherian, J.J., Kapadia, B.H., Banerjee, S., Jauregui, J.J., Issa, K., Mont, M.A., 2014. Mechanical, anatomical, and kinematic axis in TKA: Concepts and practical applications. Curr. Rev. Musculoskelet. Med. 7, 89-95.

Culvenor, A.G., Perraton, L., Guermazi, A., Bryant, A.L., Whitehead, T.S., Morris, H.G., Crossley, K.M., 2016. Knee kinematics and kinetics are associated with early patellofemoral osteoarthritis following anterior cruciate ligament reconstruction. Osteoarthritis Cartilage 24, 1548-1553.

D'Errico, J., 2007. Graphical data selection tool, MATLAB Central File Exchange.

Grood, E.S., Suntay, W.J., 1983. A joint coordinate system for the clinical description of three-dimensional motions: Application to the knee. J. Biomech. Eng. 105, 136-144.

Gu, Y., Roth, J.D., Howell, S.M., Hull, M.L., 2014. How frequently do four methods for mechanically aligning a total knee arthroplasty cause collateral ligament imbalance and change alignment from normal in white patients? AAOS exhibit selection. J. Bone Joint Surg. Am. 96, e101.

Indrayan, A., 2013. Methods of clinical epidemiology, Springer series on epidemiology and public health. Springer-Verlag, Berlin, Heidelberg, p. 24.

Lozano, R., Howell, S.M., Hull, M.L., 2019. Repeatability, reproducibility, and agreement of three computational methods to approximate the functional flexion-extension axis of the tibiofemoral joint using 3D bone models of the femur. Comput. Methods Biomech. Biomed. Engin. 22, 1144-1152.

Luo, C.F., 2004. Reference axes for reconstruction of the knee. Knee 11, 251-257.

Marchant, D.C., Rimmington, D.P., Crawford, R.W., Whitehouse, S.L., McGuire, J., 2005. An algorithm for locating the center of the ankle joint in knee navigation surgery. Comput. Aided Surg. 10, 45-49.

Martin Bland, J., Altman, D.G., 1986. Statistical Methods for Assessing Agreement Between Two Methods of Clinical Measurement. Lancet 327, 307-310.

Nicolet-Petersen, S., Saiz, A., Shelton, T., Howell, S.M., Hull, M.L., 2020. Small differences in tibial contact locations following kinematically aligned TKA from the native contralateral knee. Knee Surg. Sports Traumatol. Arthrosc. 28, 2893-2904.

Pinskerova, V., Johal, P., Nakagawa, S., Sosna, A., Williams, A., Gedroyc, W., Freeman, M.A.R., 2004. Does the femur roll-back with flexion? J. Bone. Jt. Surg. - Ser. B. 86, 925-931.

Siston, R.A., Daub, A.C., Giori, N.J., Goodman, S.B., Delp, S.L., 2005. Evaluation of methods that locate the center of the ankle for computer-assisted total knee arthroplasty. Clin. Orthop. Relat. Res. 439, 129-135.

Subburaj, K., Ravi, B., Agarwal, M., 2010. Computer-aided methods for assessing lower limb deformities in orthopaedic surgery planning. Comput. Med. Imaging Graph. 34, 277-288.

Yoo, J.H., Chang, C.B., Shin, K.S., Seong, S.C., Kim, T.K., 2008. Anatomical references to assess the posterior tibial slope in total knee arthroplasty: A comparison of 5 anatomical axes. J. Arthroplasty 23, 586-592.

Yoshioka, Y., Siu, D.W., Scudamore, R.A., Cooke, T.D.V., 1989. Tibial anatomy and functional axes. J. Orthop. Res. 7, 132-137.

FIGURES/TABLES

Table 1.1. Intraobserver (repeatability) and interobserver (reproducibility) interclass coefficients (ICCs) for each method of finding the center of the talocrural joint.

	Diagonal Intersection Method	Area Centroid Method	Biplanar Method
Repeatability			
ML Coordinate	0.71	0.98	0.96
AP Coordinate	0.91	0.97	0.86
PD Coordinate	0.98	0.98	0.99
Reproducibility			
ML Coordinate	0.46	0.92	0.77
AP Coordinate	0.56	0.94	0.40
PD Coordinate	0.96	0.96	0.90

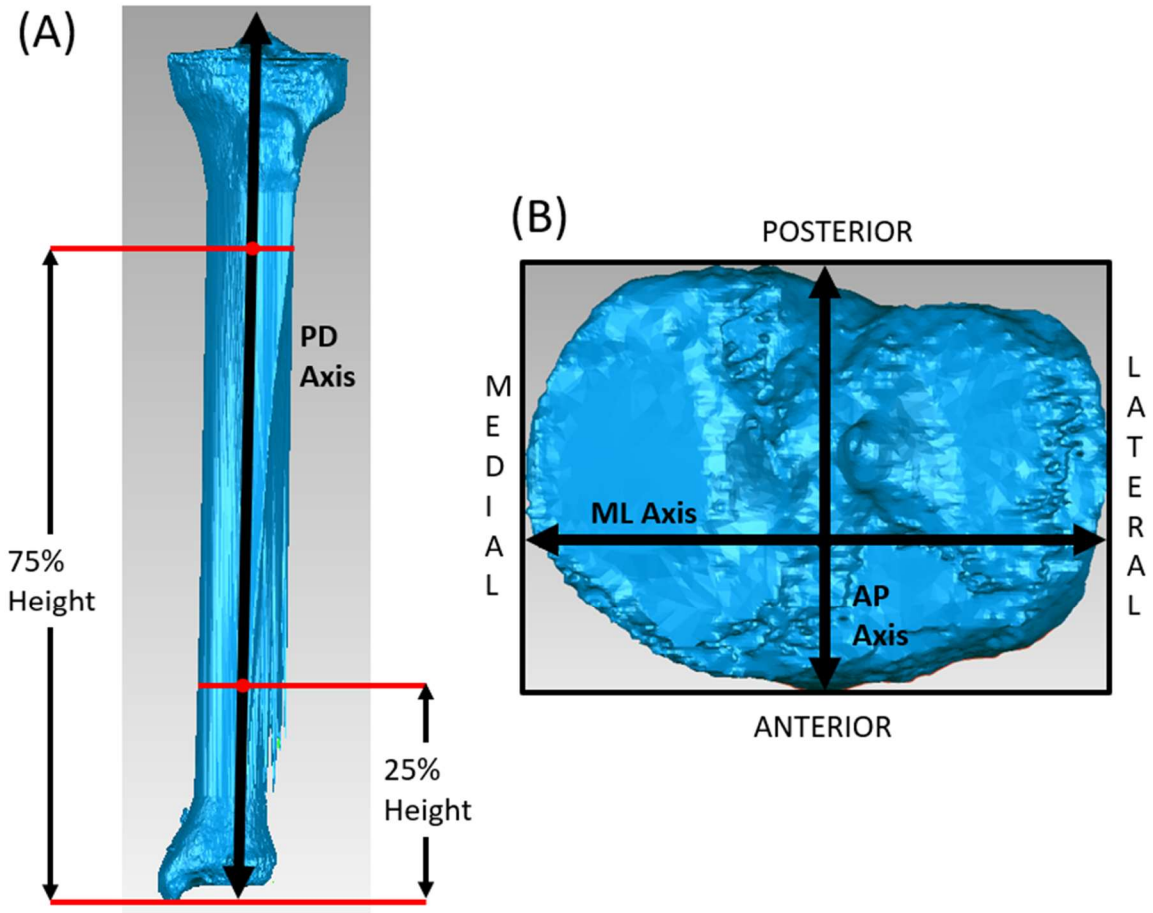

Figure 1.1. Configuration of the tibial coordinate system for a 3D tibia model. (A) The PD axis was established by connecting the centroids of two tibial shaft cross-sections. The bone height was computed by finding the distance between the most inferior point on the medial malleolus and the most superior point on the intercondylar eminences. The first cross-section was located a quarter of the bone height above the most inferior point on the medial malleolus, and the second cross-section was located three-quarters of the bone height above the most inferior point on the medial malleolus. (B) The bounding box around the tibial plateau defined the directions of the AP and ML axes. The PD axis extended out-of-plane at the intersection of the AP and ML axes. For a left knee, anterior, lateral, and proximal directions were positive.

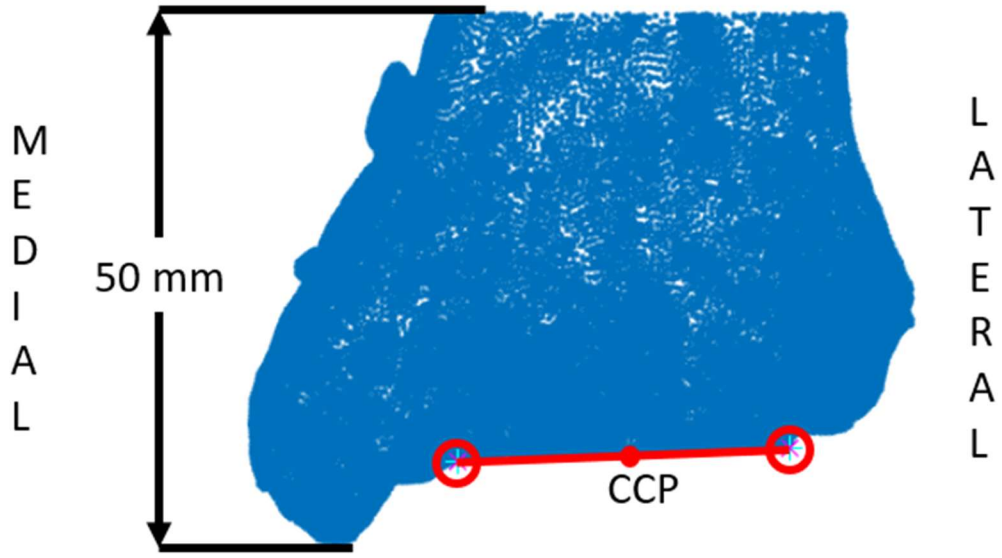

Figure 1.2. The distal tibia point cloud in coronal view. The red circles show the two selected points representing the medial and lateral edges of the distal weight-bearing articular surface. The medial edge is found at the start of the flat section where the medial malleolus ends, and the lateral edge is found at the end of the flat section where the bone begins to curve upward. The midpoint of the line connecting the two edges was defined as the coronal center point (CCP).

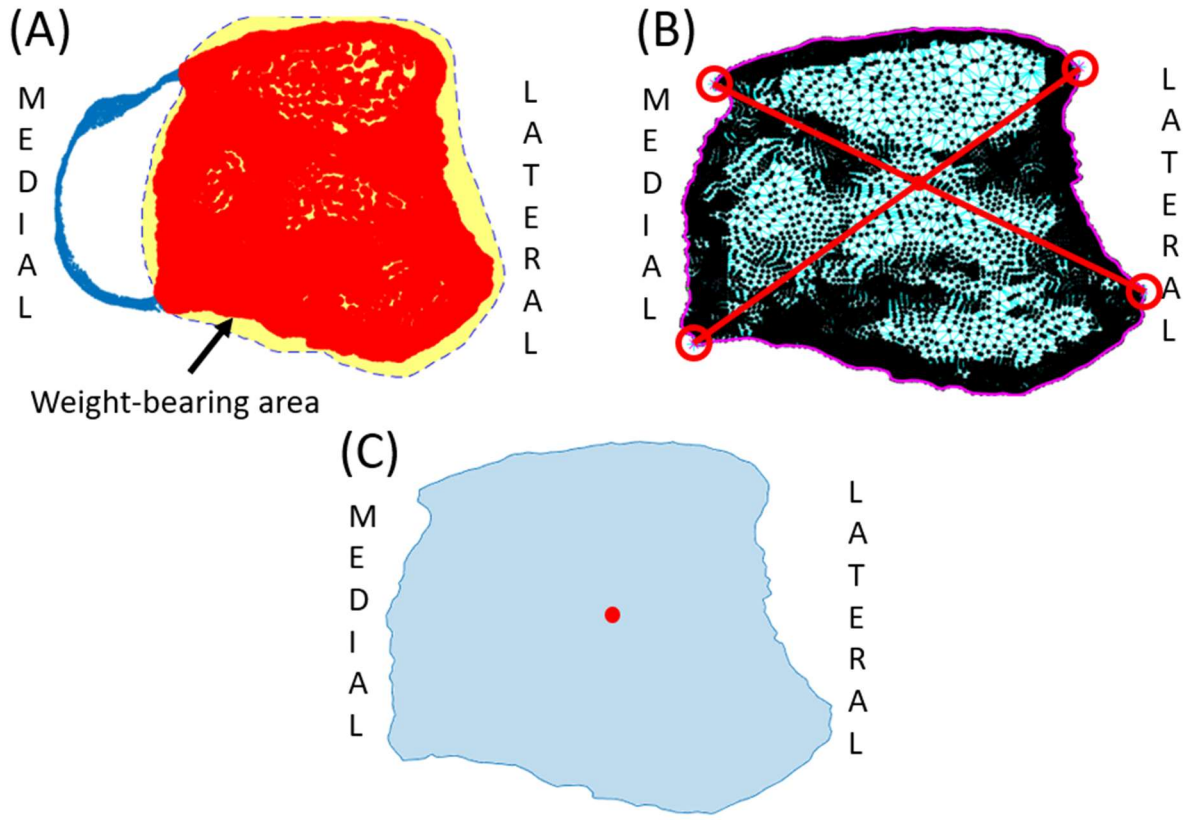

Figure 1.3. Axial view of points that were within 1 mm below and within 6 mm above the coronal center point. (A) The weight-bearing area of the distal articular surface was isolated using a lasso selection program. (B) The boundary-extraction code produced a contour (magenta) of the weight-bearing area. The red circles show the four selected points representing the corners of the weight-bearing distal articular surface. These four points were chosen such that a resulting quadrilateral determined by connecting the points would approximate the weight-bearing area of the distal articular surface. The diagonal intersection method defines the center of the talocrural joint as the intersection of two diagonals drawn from the corner points. (C) The area centroid method defines the center of the talocrural joint as the centroid (red dot) of the weight-bearing area (shaded blue).

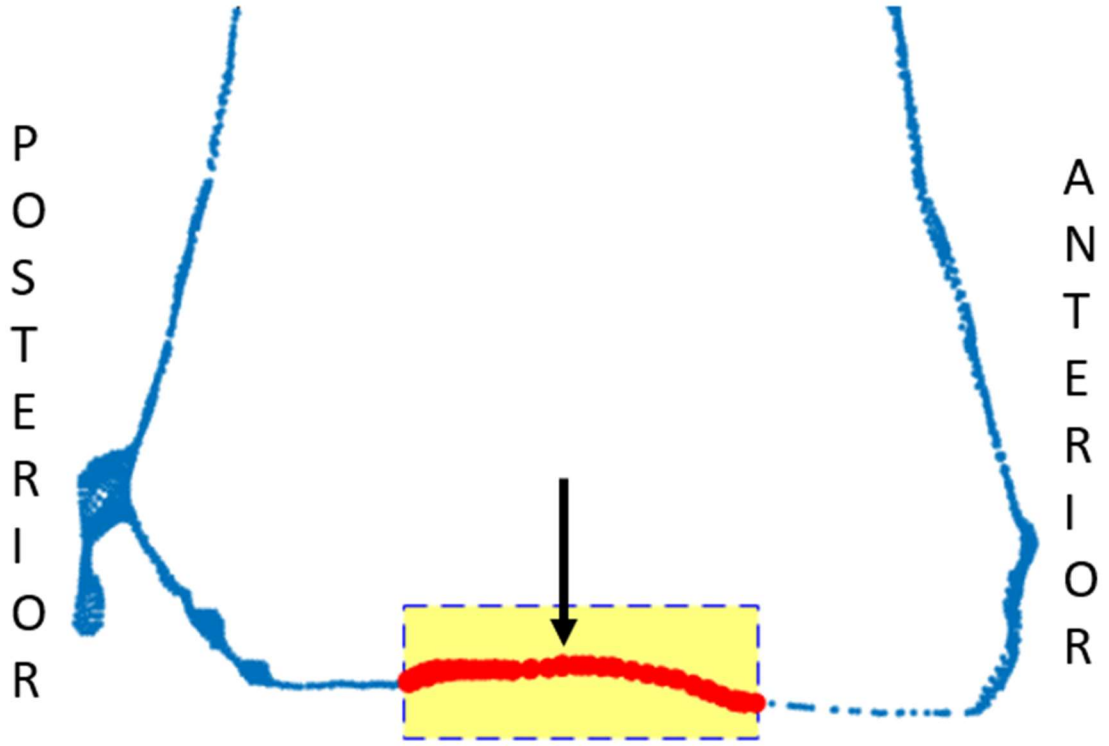

Figure 1.4. Cross-section of the isolated distal tibia in sagittal view. The highest point within the selected yellow region (depicted by the black arrow) represents the peak of the distal articular surface.

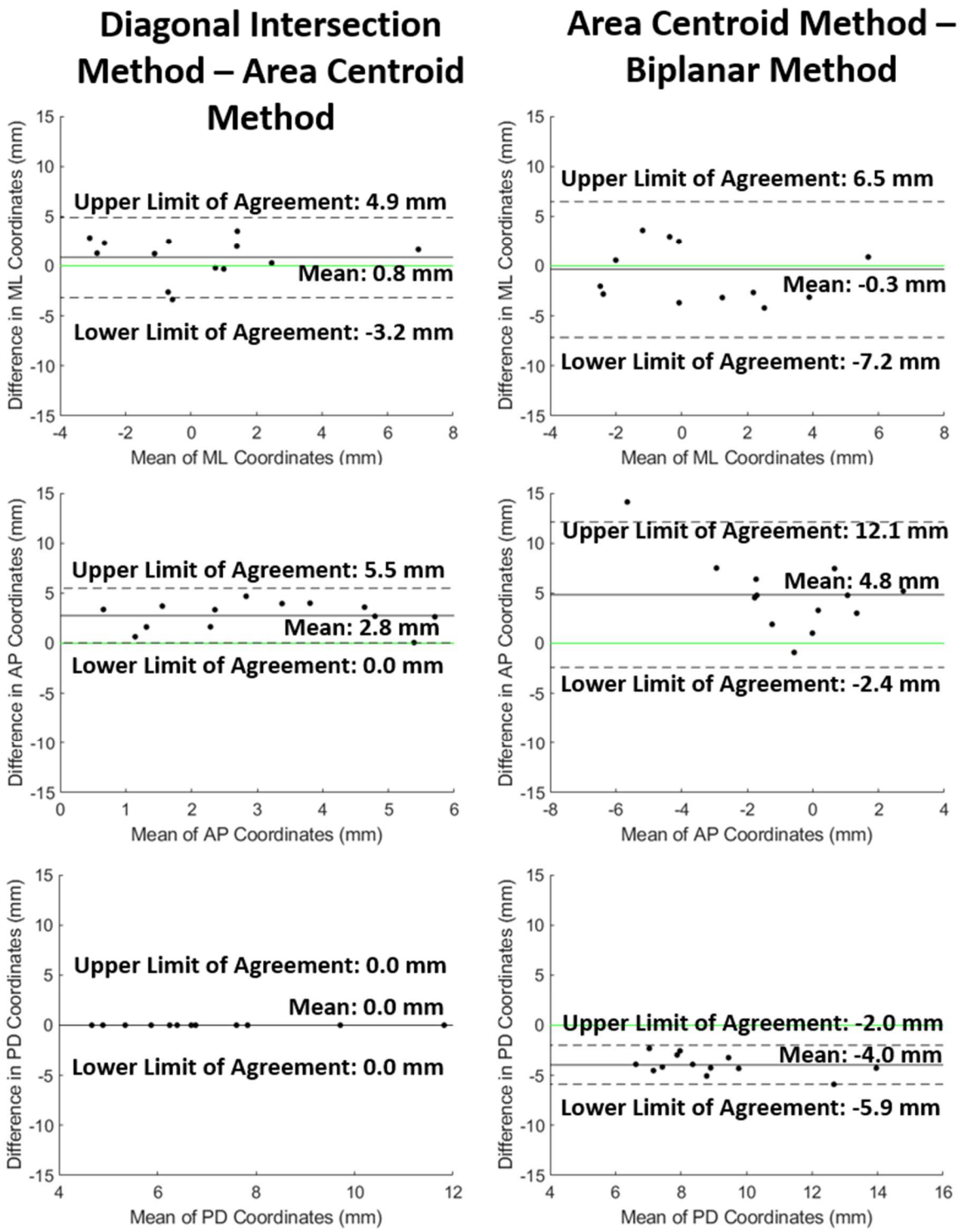

Figure 1.5. Bland-Altman plots comparing differences in center coordinates of the talocrural joint for two pairs of methods and limits of agreement.

Chapter 2: Agreement Between Two Methods for Computing the Anterior-Posterior Positions of Native Femoral Condyles Using 3D Bone Models With and Without Articular Cartilage and Smoothing

ABSTRACT

Background: Knowledge of anterior-posterior (AP) movement of the femoral condyles on the tibia in the native (i.e. healthy) knee provides an objective measurement of tibiofemoral kinematics, which would serve to assess whether an artificial knee restores natural movement. Two common methods for identifying AP positions and hence condylar movements include: 1) the flexion facet center (FFC), and 2) the lowest point (LP) methods. The objectives were to 1) determine how well the two methods agree, and 2) determine whether the addition of articular cartilage and/or smoothing significantly affects AP positions.

Methods: Magnetic Resonance (MR) images of the native knee were obtained from eleven subjects, who subsequently performed a deep knee bend under fluoroscopy. For each subject, four different MR models of the distal femur were created: femur bone, smoothed femur bone, femur bone with cartilage, and femur bone with smoothed cartilage. AP positions of the LPs and FFCs in each compartment were determined for each model type following 3D model-to-2D image registration.

Results: In the medial and lateral compartments for the femur bone with smoothed cartilage at 0° flexion, mean AP positions of the LPs were 7.7 mm and 5.4 mm more anterior than those of the FFCs, respectively ($p < 0.0001$, $p = 0.0002$) and limits of agreement were ± 5.5 mm. At 30°, 60°, and 90° flexion, the difference in mean AP positions was 1.5 mm or less even when significant and the limits of agreement were bounded by ± 2.4 mm. Differences in AP positions between model types were minimal for both LPs and FFCs.

Conclusion: In the native knee, the FFC and LP methods provided similar mean results during a deep knee bend at flexion angles of 30° and beyond but not at 0°. These results resolve a decade-old contradiction in the literature. Since addition of cartilage to 3D bone models is not required to accurately determine AP positions, faster and less expensive imaging techniques such as CT can be used confidently to acquire the 3D bone models for the analysis of tibiofemoral kinematics.

INTRODUCTION

Total knee arthroplasty (TKA) is a common treatment for tibiofemoral and patellofemoral osteoarthritis, with over 1 million procedures performed annually in the US alone (Kurtz et al., 2014). However, approximately one in five patients are reportedly dissatisfied with their outcome (Noble et al., 2006; Baker et al., 2007; Bourne et al., 2010). Patient satisfaction is strongly correlated to improved outcomes (Becker et al., 2011), and one of the desirable outcomes is restoring tibiofemoral kinematics that closely match the native (i.e. pre-arthritic) knee (Miner et al., 2003; Bourne et al., 2010; Lange et al., 2017). Hence, to improve the outcomes and in turn patient satisfaction, a thorough characterization of tibiofemoral kinematics in the native knee is a necessary foundation.

One way to measure tibiofemoral kinematics is by analyzing the movement of anterior-posterior (AP) positions of the femoral condyles with respect to the tibia during activities of daily living. As the knee flexes, the AP positions of the femoral condyles can be determined at specified flexion angles, which can be used to track the individual movement of each condyle (Asano et al., 2001; Pinskerova et al., 2004). Knowing the movements of the condyles also allows for measurement of internal-external (IE) rotation of the femur with respect to the tibia (Iwaki et al., 2000; Asano et al., 2001). By determining these movements in the native knee, a comparison can be made with the movements of condyles following TKA to assess the degree to which TKA kinematics are restored to native (Nicolet-Petersen et al., 2019). Because contact between the tibia and femur is not lost during active flexion (Martelli et al., 2002), because compressive deformation of the articular cartilage is small (Eckstein et al., 2005), and because medial-lateral displacement is of limited clinical interest (Blankevoort et al., 1988), AP movements of the femoral condyles provide a comprehensive picture of tibiofemoral kinematics in the native knee.

There are two primary methods for identifying the AP positions of the femoral condyles. One method uses the AP position of the flexion facet center (FFC), which is the center of a circle fit to the

condyle's posterior articular surface (Iwaki et al., 2000; Asano et al., 2001; Pinskerova et al., 2004). The other method uses the lowest point (LP) on each condyle with respect to the plane parallel to the tibial articular surface (Banks et al., 1997; Hoff et al., 1998; Asano et al., 2001; Walker et al., 2011). However, comparison of AP from the two methods in the native knee yielded contradictory findings (Asano et al., 2001; Pinskerova et al., 2004; Walker et al., 2011). Two studies (Asano et al., 2001; Pinskerova et al., 2004) reported different AP positions between the two methods particularly at 0° flexion and similar AP positions later in flexion whereas the other study (Walker et al., 2011) showed similar AP positions at 0° flexion and different AP positions particularly at 90° flexion. Further, differences in AP positions were not analyzed statistically by any of these studies. To resolve this contradiction thus adding confidence to our knowledge of tibiofemoral kinematics in the native knee, our first objective was to determine how well the two methods agree. Agreement was analyzed by determining whether mean AP positions differed statistically over a flexion range of 0º - 90º and the limits of agreement. Limits of agreement are useful in capturing the 95% confidence interval of the discrepancies between methods of clinical measurement (Martin Bland & Altman, 1986).

Two factors must be considered before applying the FFC and LP methods. The first factor is the presence of cartilage on the 3D model of the femur. Cartilage thickness varies across different regions of the femoral condyles (DeFrate et al., 2004; Li et al., 2005; Koo et al., 2011) so that the addition of cartilage to the 3D bone model of the femur can alter the shape of the posterior condylar surface. Since methods for determining the FFCs rely on best fit of geometric primitives such as circles (Iwaki et al., 2000; Asano et al., 2001; Most et al., 2004; Freeman and Pinskerova, 2005; McPherson et al., 2005; Kozanek et al., 2009; Leszko et al., 2011; Walker et al., 2011), cylinders (Gray et al., 2020), or spheres (Tanifuji et al., 2011; Yin et al., 2015) to the femoral articular surfaces and since the LPs depend on the shape of the femoral articular surfaces, the results of both methods might be affected by the inclusion of articular cartilage. Although one study found that addition of cartilage improves

accuracy of condylar AP positions for the LP method (DeFrate et al., 2004), no similar study has been performed for the FFC method.

Another factor to consider is the smoothness of the 3D model. Noise artifacts are present in 3D models created from segmented images, which result in distortions and rough surfaces, especially in models generated from MR images (White et al., 2008). To mitigate these artifacts, the surfaces of the 3D models can be smoothed in a post-processing low-pass filtering operation. However, the effects of smoothing on the AP positions of the femoral condyles have not been investigated for either the FFC or LP methods.

A second objective of this study was to determine whether the addition of cartilage and/or smoothing significantly affects the AP positions of the femoral condyles for both the FFC and LP methods. Based on these results, a gold standard 3D femoral model could be established for future studies measuring the femoral condyle AP positions.

METHODS

Data Collection

Eleven TKA patients were selected from a group of subjects, all of whom had no skeletal abnormalities or prior surgery in the native contralateral limb and were able to perform activities of daily living without discomfort in the native contralateral limb. Each patient performed a deep knee bend from full extension to maximum flexion while fluoroscopic images (OEC 9900 Elite, General Electric, Boston, MA) were obtained for each subject's native knee in an anterior oblique sagittal orientation of about 10° – 15° at 15 frames per second (Nicolet-Petersen et al., 2019). For the deep knee bend, patients staggered their stance in the AP direction to prevent the contralateral knee from impeding the view of the knee under study, and to keep both feet planted on the platform. Patients performed the activities over 5-7 s to reduce motion blur and handrails were provided to aid in stability. Afterwards, each native knee was imaged with a 3T MRI (TIM Trio, Siemens, Munich,

Germany) with 1 mm thick sagittal plane slices (flip angle = 12°, 256 × 256 pixel resolution interpolated to 512 × 512, 0.8 × 0.8 × 1.0 mm voxel size, TR = 17 ms, TE = 4 ms), and the resulting MR images were segmented using commercially available software (Mimics v20.0, Materialise, Belgium) to create 3D models of the distal femur, proximal tibia, and femoral articular cartilage.

Data Processing

Fluoroscopic images at 0°, 30°, 60°, and 90° flexion were identified for the deep knee bend, and the in vivo 3D position and orientation of the MR bone models were determined using 3D model-to-2D image registration techniques (Banks & Hodge, 1996) and open-source software (https://sourceforge.net/projects/jointtrack/). Bone models were projected onto the fluoroscopic images and repeatedly adjusted in six degrees of freedom until the model silhouettes closely matched the bone silhouettes in the image. Finally, the femur was translated in the out-of-plane direction until it was centered over the tibia. This step was necessary given that the out-of-plane translation errors encountered in single-plane fluoroscopy can result in the reconstruction of physiologically impossible poses (Fregly et al., 2005; Prins et al., 2010).

A coordinate system was defined on the plane perpendicular to the mechanical axis of the tibia to report the AP femoral condyle positions. To obtain the tibial mechanical axis, a 3D bone model of each subject's full native tibia was created from thin slice (1.25 mm) computed tomography (CT) images obtained from post-operative CT scanograms. CT images were obtained following the Perth Protocol, and the CT tibia bone models were constructed using open-source software (3D Slicer version 4.10.0). Next, the MR and CT bone models were imported into commercial software (Geomagic Control, 3D Systems, Cary, NC), where the CT tibia models were registered to the MR tibia models. The tibial mechanical axis was constructed using the CT tibia model by drawing a line from the centroid of the tibial articular surface of the talocrural joint to the midpoint between the intercondylar eminences. The axial plane was set perpendicular to the tibial mechanical axis. The

origin of the tibial coordinate system was defined by the center of the bounding box drawn around the tibial plateau (Figure 2.1).

Once the tibial coordinate system was established, four different types of MR models for the distal femur were created for each patient (Figure 2.2). The first type was a 3D bone model of the femur, and the second type was a 3D bone model of the femur with femoral articular cartilage. The third and fourth model types were similar to the first two types, but with the surfaces of the 3D models smoothed in commercial software (Geomagic Control 2015, 3D Systems, Cary, NC). Smoothing was performed using the commercial software's "Reduce Noise" tool (Parameters: Prismatic shapes (conservative), Smoothness Level = 4 (Max), Iterations = 1, Deviation Limit = 9.0176 mm) such that noise was largely removed while preserving the overall shapes of the femoral condyles.

The AP femoral condyle positions in the medial and lateral compartments for the native knee were determined for each MR model type and flexion angle using both the LP and FFC methods. The LP was defined as the geometric centroid of all points on the condyle within 0.5 mm above the point on the condyle nearest to the plane perpendicular to the tibial mechanical axis. The FFC of each femoral condyle was determined by finding the center of the best-fit single circle for the sagittal projection of the femoral condyle for 10° – 110° of flexion (Figure 2.3). The sagittal projections were obtained by superimposing the posterior femoral condyles of the 3D femur bone model. AP femoral condyle positions were standardized to the average AP dimension of all native tibial plateaus (55.2 mm) by multiplying each subject's AP condyle positions by the ratio of the average AP dimension of all native tibial plateaus to the AP dimension of their native tibial plateau.

To accurately define the FFC, a 0º flexion reference was established for each patient by rotating the femur and tibia models such that their mechanical axes were vertically oriented and parallel in the sagittal view. The femoral mechanical axis was found by defining the femoral anatomical axis in the sagittal view as the line connecting the midpoint of the proximal end of the

femoral shaft (10 cm above the joint line) and the apex of the intercondylar notch, then rotating the femoral anatomical axis 3.0° about the intercondylar notch such that the proximal end moved anterior (Chung et al., 2009). The tibial mechanical axis was found by defining the line along the anterior tibial cortex in the sagittal view as the line connecting the tibial tubercle and the most anterior point on the distal end of the tibial shaft (15 cm below the tubercle), then rotating the anterior tibial cortex line 2.2° about the tibial tubercle such that the distal end moved anterior (Han et al., 2008).

Statistical Analysis

The mean and standard deviation were computed to describe the AP femoral condyle positions in the medial and lateral compartments at each flexion angle for each model type. To determine whether mean AP femoral condyle positions differed between the LP and FFC methods, a two-factor analysis of variance (ANOVA) with repeated measures was performed for each of the medial and lateral compartments using the AP femoral condyle positions for the smooth 3D femur bone-cartilage models. The two factors were method at two levels and flexion angle at four levels. Since significant and important interactions were apparent, post hoc analyses consisted of paired t-tests at each flexion angle. Agreement between the LP and FFC methods was quantified by constructing Bland-Altman plots and determining limits of agreement (Martin Bland & Altman, 1986).

To determine whether model type affected mean AP positions, a two-factor analysis of ANOVA with repeated measures was performed for each of the medial and lateral compartments and for each method (i.e. four ANOVAs) where the two factors were the model type at four levels and flexion angle at four levels (JMP, SAS Institute Inc., Cary, NC). When significant and important interactions were apparent, single-factor repeated measures ANOVAs were performed at each flexion angle. Significance was set at $p < 0.05$.

RESULTS

In the medial and lateral compartments for the smooth 3D femur bone model with cartilage at 0° flexion, the mean AP positions of the LPs were 7.7 mm and 5.4 mm more anterior than those of the FFCs, respectively ($p \leq 0.0001$, $p = 0.0002$). At 30°, 60°, and 90° flexion, the difference in the mean AP positions was 1.5 mm or less even when statistically significant (medial compartment 30° and 60°: $p \leq 0.0111$; lateral compartment 90°: $p = 0.0041$) (Figure 2.4).

Referring to the Bland-Altman plots (Figure 2.5), limits of agreement were widest for 0° flexion at approximately ± 5.5 mm in both compartments. Limits of agreement were narrower at 30°, 60°, and 90° flexion with the widest interval being ± 2.4 mm for the lateral compartment at 30º flexion.

The effect of model type on AP positions was minimal (Figure 2.6). Considering first the LPs, mean AP positions in the medial compartment remained at 5 mm posterior for all model types ($p = 0.0911$ from two-factor ANOVA). In the lateral compartment, mean AP positions moved from approximately 2.5 mm posterior at 0° flexion to 10 mm posterior at 30° flexion, then remained at 10 mm posterior from 30° to 90° flexion. At 0º and 60° flexion, mean AP positions between model types differed significantly ($p \leq 0.0029$ from one factor ANOVAs) but these differences were less than 1.3 mm. At the remaining flexion angles, mean AP positions were unaffected by model types ($p \geq 0.0776$ from one factor ANOVAs).

Considering next the FFCs, mean AP positions in the medial compartment moved from 11 mm posterior at 0° flexion, to 7 mm posterior at 30° flexion, to 4 mm posterior at 60° flexion, then remained at 4 mm posterior from 60° to 90° flexion for all model types ($p = 0.6036$ from two-factor ANOVA) (Figure 2.6). In the lateral compartment, mean AP positions moved from 8 mm posterior at 0º flexion to 10 mm posterior at 30° flexion, then remained at 10 mm posterior from 30° to 90° flexion for all model types ($p = 0.1724$ from two-factor ANOVA).

DISCUSSION

To resolve the contradiction in the literature noted in the Introduction thus adding confidence to our knowledge of tibiofemoral kinematics in the native knee, our first objective was to determine whether mean AP positions differed statistically between the two methods over a flexion range of 0º - 90º and the limits of agreement. A second objective was to determine whether the addition of cartilage and/or smoothing significantly affected condylar AP positions for both the FFC and LP methods, with the goal of establishing a gold standard 3D femoral model for future studies measuring the AP positions. Related to the first objective, one key finding was that FFC and LP methods yielded similar AP positions during a deep knee bend at flexion angles of 30° and beyond but not at 0º. A second key finding was that model type minimally affect the AP positions of the femoral condyles for both the FFC and LP methods.

The present study has shown that the FFC and LP methods yield significantly different AP positions of the femoral condyles at 0° flexion during a deep knee bend. The large mean differences (7.7 mm and 5.4 mm) and wide limits of agreement (± 5.5 mm) between the LPs and FFCs in the medial and lateral compartments, respectively, can be attributed to the sagittal profiles of the native femoral condyles being non-circular at full extension. For flexion angles in the range 10°-110°, the profiles of posterior femoral condyles are well approximated by single circles (Asano et al., 2005; Yin et al., 2015), which results in the FFC and LP sharing the same AP position (Asano et al., 2001). At 0° flexion however, the profiles are no longer well approximated by single circles due to a decrease in curvature and corresponding increase in radius of curvature, so that the FFC was significantly more posterior than the LP (Figure 2.4) (Asano et al., 2001; Pinskerova et al., 2004).

At 30°, 60°, and 90° flexion, differences in mean AP positions between the LPs and FFCs were 1.5 mm or less for both medial and lateral compartments, even when significant. The limits of agreement also show that the differences in AP positions between the LPs and FFCs did not exceed ±

2.4 mm in 95% of subjects. However, none of these differences may be clinically important in the context of their relationship to the 55 mm average AP dimension of all native tibial plateaus because these differences are approximately 5% or less. Hence, it can be concluded that the FFC and LP methods yield the similar AP positions of the femoral condyles for flexion angles at 30° and beyond, which is consistent with previous findings (Asano et al., 2001; Pinskerova et al., 2004).

The contradictory results of our study to those of another study (Walker et al., 2011) are difficult to explain particularly at 0° flexion. Our results as well those of Asano (2001) and Pinskerova (2004) were based on analysis of images taken under weight bearing conditions. In contrast, the results of Walker (2011) were based on 3D motion analysis of cadaveric knee specimens loaded with a small non-physiologic compressive load of 74 N and the quadriceps tendon loaded to set the desired flexion angle. Even though the loading was different, the mechanism (i.e. increase in radius of curvature going from 30º to 0º of flexion) responsible for the different AP positions between LPs and FFCs should not have been affected. In any case, the preponderance of the evidence indicates that the AP positions of the LPs and FFCs differ at 0° of flexion but are similar at 30º of flexion and beyond.

For the FFC method, the model type had no significant effect on the AP positions of the femoral condyles for both medial and lateral compartments. The lack of significant differences between model types can be attributed to the circle-fitting process used to define the FFC. The best-fit single circle was defined such that the resulting fit minimized the relative root-mean-squared radial deviation from the sagittal profile of the posterior condyle, which diminished the effect of noise on the 3D model surface. Therefore, smoothing the model did not significantly alter the radius and center of the best-fit single circle. Meanwhile, the addition of cartilage was expected to increase the radius of the best-fit single circle but have no significant effect on the circle's center. Therefore, cartilage inclusion did not change the AP position of the FFC.

Likewise for the LP method, the model type had no significant effect on the AP positions of the femoral condyles for both medial and lateral compartments. The lack of significant differences between the smoothed and non-smoothed models can be attributed to the LP's definition as a geometric centroid. For a cluster of points on the femoral condyle, the geometric centroid was defined as the mean of all points within the cluster. This averaging process diminished the effect of noise on the 3D model surface, so that smoothing the model did not significantly alter the AP position of the LP.

The lack of significant differences between the bone and bone with cartilage models was surprising, since previous studies have found that in the lateral compartment at 0° flexion the LP changed significantly when cartilage was added (DeFrate et al., 2004). This discrepancy can be attributed to the accuracy of cartilage thickness for MR-based models. For thinner regions of femoral cartilage, the cartilage thickness on the MR-based models is overestimated (Koo et al., 2009). On the lateral femoral condyle, the thinnest region of cartilage is at 0° flexion where cartilage-to-cartilage contact is minimal (Li et al., 2005). Hence, the femoral cartilage thickness at 0° flexion will be overestimated and appear thicker on the MR-based model. Another study showed that for MR-models constructed from two different 3.0T MRI scanners, the average femoral cartilage thickness did not vary significantly with flexion (Kornaat et al., 2006). Based on these studies, variations in femoral cartilage thickness on the MR-based models were not large enough to affect the AP position of the LP when cartilage was added to a bone model.

Our finding that AP positions were similar between model types for both FFCs and LPs is useful for two reasons. One reason is that addition of cartilage to the 3D bone models of the femur and tibia is not required to accurately measure AP positions. Hence, faster and less expensive imaging techniques such as CT can be used confidently instead of MRI to acquire the 3D bone models for the analysis of tibiofemoral kinematics. Use of CT scans is advantageous because they can be acquired

significantly faster than MRI scans (Bushberg et al., 2013), are approximately half the cost (Ibrahim et al., 2012; Rehana et al., 2013), and have been used extensively to create 3D bone models for the analysis of tibiofemoral kinematics (Asano et al., 2001; Fregly et al., 2005; You et al., 2001). A further advantage of CT scans is that outlines of CT-derived 3D bone models correspond better with single-plane fluoroscopic projections than outlines of the MR-derived models (Moro-oka et al., 2007), making CT-derived models the superior choice for 3D model-to-2D image registration. A second usefulness is that our results lend confidence in both the FFC and LP methods and the tibiofemoral kinematics derived from such. Because two fundamentally different methods provided similar results, the results from one method validated the results from the other. This validation bolsters confidence in our knowledge of tibiofemoral kinematics in the native knee.

One methodological issue which affected our results was the reference plane selected for analysis. In our study, the plane perpendicular to the tibial mechanical axis was selected. Most studies within the literature however used the plane parallel to the tibial plateau (Asano et al., 2001; DeFrate et al., 2004; Walker et al., 2011). The plane perpendicular to the tibial mechanical axis was selected for two reasons. One reason was that the goal of determining AP positions of the femoral condyles is to quantify tibiofemoral kinematics. Choosing a plane perpendicular to the tibial mechanical axis allowed the AP positions to be expressed in a direction consistent with the coordinate system of Grood and Suntay (Grood and Suntay, 1983) where the AP direction is along the floating axis. Since the floating axis is mutually perpendicular to the flexion-extension (FE) axis body-fixed to the femur and the internal-external (IE) rotation axis body-fixed to the tibia and since the IE axis closely parallels the tibial mechanical axis (Churchill et al., 1998), the plane perpendicular to the mechanical axis is the plane parallel to the floating axis.

A second methodological issue which affected our results concerned the range of flexion over which a single circle was fit to determine the FFC of each femoral condyle. Although qualitatively

circles fit the profiles well over the flexion range 10º - 110º (Figure 2.3), detailed quantitative examinations of the femoral condyle saggital profiles revealed variations in the radius of curvature (Rostlund et al., 1989; Nuno et al., 2003; Kosel et al., 2010). Since the AP positions of the LPs and FFCs are identical so long as the profiles have a constant radius of curvature (i.e. are circular) (Asano et al., 2001; Simileysky et al., 2021), differences between the AP positions occurred because of variations in the radius of curvature along the profile in the flexion range analyzed. Better agreement in the AP positions provided by the two methods would have occurred if the FFCs reflected the instantaneous radius of curvature. In this case, differences would have been negligible. However, the FFCs would not have a fixed position on the femoral condyles thus complicating the determination of flexion-extension (FE) axis of rotation. Inasmuch as FFCs identified by geometric primitives such as circles (Iwaki et al., 2000; Asano et al., 2001; Most et al., 2004; Freeman and Pinskerova, 2005; McPherson et al., 2005; Kozanek et al., 2009; Leszko et al., 2011; Walker et al., 2011), cylinders (Eckhoff et al., 2005; Gray et al., 2019) and spheres (Tanafuji et al., 2011; Yin et al., 2015) fit to this range of flexion have been common in the literature, our interest focused on differences in the AP positions between the two methods for single circles fit to this flexion range.

CONCLUSION

This study statistically analyzed AP positions of the femoral condyles in the native knee as indicated by the FFC and LP methods and concluded that AP positions are similar during a deep knee bend for flexion angles of 30° and beyond but differ at 0° of flexion. Thus, our results resolve contradictory results in the literature which have stood for at least a decade thus adding confidence to our knowledge of tibiofemoral mechanics in the native knee. Since model types only minimally affected AP positions of the LPs and FFCs, addition of cartilage to the 3D bone models of the femur and tibia is not required to accurately measure the AP positions of the condyles. Hence, faster and less

costly imaging techniques such as CT can be used confidently instead of MRI to acquire 3D bone models for the analysis of tibiofemoral kinematics.

ACKNOWLEDGMENT

The authors are grateful to Medacta USA, Inc. for financial support.

REFERENCES

Asano, T., Akagi, M., Nakamura, T., 2005. The functional flexion-extension axis of the knee corresponds to the surgical epicondylar axis: In vivo analysis using a biplanar image-matching technique. J. Arthroplasty 20, 1060-1067.

Asano, T., Akagi, M., Tanaka, K., Tamura, J., Nakamura, T., 2001. In vivo three-dimensional knee kinematics using a biplanar image-matching technique. Clin. Orthop. Relat. Res. 388, 157-166.

Baker, P.N., van der Meulen, J.H., Lewsey, J., Gregg, P.J., 2007. The role of pain and function in determining patient satisfaction after total knee replacement. Data from the national joint registry for England and Wales. J. Bone. Jt. Surg. - Ser. B. 89, 893-900.

Banks, S.A., Hodge, W.A., 1996. Accurate measurement of three-dimensional knee replacement kinematics using single-plane fluoroscopy. IEEE Trans. Biomed. Eng. 43, 638-649.

Banks, S.A., Markovich, G.D., Hodge, W.A., 1997. In vivo kinematics of cruciate-retaining and -substituting knee arthroplasties. J. Arthroplasty 12, 297-304.

Becker, R., Döring, C., Denecke, A., Brosz, M., 2011. Expectation, satisfaction and clinical outcome of patients after total knee arthroplasty. Knee Surg. Sports Traumatol. Arthrosc. 19, 1433-1441.

Blankevoort, L., Huiskes, R., de Lange, A., 1988. The envelope of passive knee joint motion. J. Biomech. 21, 705-709,711-720.

Bourne, R.B., Chesworth, B.M., Davis, A.M., Mahomed, N.N., Charron, K.D.J., 2010. Patient satisfaction after total knee arthroplasty: Who is satisfied and who is not? Clin. Orthop. Relat. Res. 468, 57-63.

Bushberg, J.T., Seibert, J.A., Leidholdt, E.M., Boone, J.M., 2012. The Essential Physics of Medical Imaging, 3rd ed. Lippincott Wiliams and Wilkins, Philadelphia, PA, USA.

Chung, B.J., Kang, Y.G., Chang, C.B., Kim, S.J., Kim, T.K., 2009. Differences between sagittal femoral mechanical and distal reference axes should be considered in navigated TKA. Clin. Orthop. Relat. Res. 467, 2403-2413.

Churchill, D.L., Incavo, S.J., Johnson, C.C., Beynnon, B.D., 1998. The transepicondylar axis approximates the optimal flexion axis of the knee. Clin. Orthop. Relat. Res. 356, 111-118.

Defrate, L.E., Sun, H., Gill, T.J., Rubash, H.E., Li, G., 2004. In vivo tibiofemoral contact analysis using 3D MRI-based knee models. J. Biomech. 37, 1499-1504.

Eckhoff, D.G., Bach, J.M., Spitzer, V.M., Reinig, K.D., Bagur, M.M., Baldini, T.H., Flannery, N.M.P., 2005. Three-dimensional mechanics, kinematics, and morphology of the knee viewed in virtual reality. J. Bone Joint Surg. 87, 71-80.

Eckstein, F., Lemberger, B., Gratzke, C., Hudelmaier, M., Glaser, C., Englmeier, K.H., Reiser, M., 2005. In vivo cartilage deformation after different types of actvity and its dependence on physical training status. Ann. Rheum. Dis. 64, 291-295.

Freeman, M.A.R., Pinskerova, V., 2005. The movement of the normal tibio-femoral joint. J. Biomech. 38, 197-208.

Fregly, B.J., Rahman, H.A., Banks, S.A., 2005. Theoretical accuracy of model-based shape matching for measuring natural knee kinematics with single-plane fluoroscopy. J. Biomech. Eng. 127, 692-699.

Gray, H.A., Guan, S., Thomeer, L.T., Schache, A.G., de Steiger, R., Pandy, M.G., 2019. Three-dimensional motion of the knee-joint complex during normal walking revealed by mobile biplane x-ray imaging. J. Orthop. Res. 37, 615-630.

Gray, H.A., Guan, S., Young, T.J., Dowsey, M.M., Choong, P.F., Pandy, M.G., 2020. Comparison of posterior-stabilized, cruciate-retaining, and medial-stabilized knee implant motion during gait. J. Orthop. Res. 38, 1753-1768.

Grood, E.S., Suntay, W.J., 1983. A joint coordinate system for the clinical description of three-dimensional motions: Application to the knee. J. Biomech. Eng. 105, 136-144.

Han, H.S., Chang, C.B., Seong, S.C., Lee, S., Lee, M.C., 2008. Evaluation of anatomic references for tibial sagittal alignment in total knee arthroplasty. Knee Surg. Sports Traumatol. Arthrosc. 16, 373-377.

Hoff, W.A., Komistek, R.D., Dennis, D.A., Gabriel, S.M., Walker, S.A., 1998. Three-dimensional determination of femoral-tibial contact positions under in vivo conditions using fluoroscopy. Clin. Biomech. 13, 455-472.

Ibrahim, R., Samian, S.d., Mazli, M., Amrizal, M., Aljunid, S.M., 2012. Cost of magnetic resonance imaging (MRI) and computed tomography (CT) scan in UKMMC. BMC Health Serv. Res. 12, P11.

Iwaki, H., Pinskerova, V., Freeman, M.A.R., 2000. Tibiofemoral movement 1: The shape and relative movements of the femur and tibia in the unloaded cadaver knee. J. Bone. Jt. Surg. - Ser. B. 82, 1189-1195.

Koo, S., Giori, N.J., Gold, G.E., Dyrby, C.O., Andriacchi, T.P., 2009. Accuracy of 3D cartilage models generated from MR images is dependent on cartilage thickness: Laser scanner based validation of in vivo cartilage. J. Biomech. Eng. 131, 121004.

Koo, S., Rylander, J.H., Andriacchi, T.P., 2011. Knee joint kinematics during walking influences the spatial cartilage thickness distribution in the knee. J. Biomech. 44, 1405-1409.

Kornaat, P.R., Koo, S., Andriacchi, T.P., Bloem, J.L., Gold, G.E., 2006. Comparison of quantitative cartilage measurements acquired on two 3.0T MRI systems from different manufacturers. J. Magn. Reson. Imaging 23, 770-773.

Kosel, J., Giouroudi, I., Scheffer, C., Dillon, E., Erasmus, P., 2010. Anatomical study of the radius and center of curvature of the distal femoral condyle. J. Biomech. Eng. 132, 091002.

Kozanek, M., Hosseini, A., Liu, F., Van de Velde, S.K., Gill, T.J., Rubash, H.E., Li, G., 2009. Tibiofemoral kinematics and condylar motion during the stance phase of gait. J. Biomech. 42, 1877-1884.

Kurtz, S.M., Ong, K.L., Lau, E., Bozic, K.J., 2014. Impact of the economic downturn on total joint replacement demand in the United States: Updated projections to 2021. J. Bone Joint Surg. Am. 96, 624-630.

Lange, T., Schmitt, J., Kopkow, C., Rataj, E., Günther, K.P., Lützner, J., 2017. What do patients expect from total knee arthroplasty? A Delphi consensus study on patient treatment goals. J. Arthroplasty 32, 2093-2099.e2091.

Leszko, F., Hovinga, K.R., Lerner, A.L., Komistek, R.D., Mahfouz, M.R., 2011. In vivo normal knee kinematics: Is ethnicity or gender an influencing factor? Clin. Orthop. Relat. Res. 469, 95-106.

Li, G., Sang, E.P., DeFrate, L.E., Schutzer, M.E., Ji, L., Gill, T.J., Rubash, H.E., 2005. The cartilage thickness distribution in the tibiofemoral joint and its correlation with cartilage-to-cartilage contact. Clin. Biomech. 20, 736-744.

Martelli, S., Pinskerova, V., 2002. The shapes of the tibial and femoral articular surfaces in relation to tibiofemoral movement. J. Bone. Jt. Surg. - Ser. B. 84, 607-613.

Martin Bland, J., Altman, D.G., 1986. Statistical methods for assessing agreement between two methods of clinical measurement. Lancet 327, 307-310.

McPherson, A., Kärrholm, J., Pinskerova, V., Sosna, A., Martelli, S., 2005. Imaging knee position using MRI, RSA/CT and 3D digitisation. J. Biomech. 38, 263-268.

Miner, A.L., Lingard, E.A., Wright, E.A., Sledge, C.B., Katz, J.N., Gillespie, W., Howie, C., Annan, I., Abernathy, P., Gibson, A., Lane, J., Pinder, I., Weir, D., Brewster, N., Bettinson, K., Needhoff, M., Jackson, R., Wilton, T., Howard, P., Forster, I., Szyprt, P., Moran, C., Whitaker, D., Bullock, M., Hinchcliffe, Z., Learmonth, I., Newman, J., Ackroyd, C., Langkamer, G., Spencer, R., Shannon, M., Smith, E., Dixon, J., Whitehouse, S., Ewald, F., Poss, R., Wright, J., Martin, S., Kwon, J., Valderrama, Y., Harwin, S., Lichardi, M., Mehlhoff, M., Weiler, L., Cahalan, T., Cronk, R., Sandago, A., Rackermann, S., McLaughlin, E., Lewis, P., Bauze, R., Stevenson, T., Morrison, G., Clasohm, J., 2003.

Knee range of motion after total knee arthroplasty: How important is this as an outcome measure? J. Arthroplasty 18, 286-294.

Moro-Oka, T.A., Hamai, S., Miura, H., Shimoto, T., Higaki, H., Fregly, B.J., Iwamoto, Y., Banks, S.A., 2008. Dynamic activity dependence of in vivo normal knee kinematics. J. Orthop. Res. 26, 428-434.

Most, E., Axe, J., Rubash, H., Li, G., 2004. Sensitivity of the knee joint kinematics calculation to selection of flexion axes. J. Biomech. 37, 1743-1748.

Nicolet-Petersen, S., Saiz, A., Shelton, T., Howell, S.M., Hull, M.L., 2020. Small differences in tibial contact locations following kinematically aligned TKA from the native contralateral knee. Knee Surg. Sports Traumatol. Arthrosc. 28, 2893-2904.

Noble, P.C., Conditt, M.A., Cook, K.F., Mathis, K.B., 2006. The John Insall Award: Patient expectations affect satisfaction with total knee arthroplasty. Clin. Orthop. Relat. Res. 452, 35-43.

Nuño, N., Ahmed, A.M., 2003. Three-dimensional morphometry of the femoral condyles. Clin. Biomech. 18, 924-932.

Pinskerova, V., Johal, P., Nakagawa, S., Sosna, A., Williams, A., Gedroyc, W., Freeman, M.A.R., 2004. Does the femur roll-back with flexion? J. Bone. Jt. Surg. - Ser. B. 86, 925-931.

Prins, A.H., Kaptein, B.L., Stoel, B.C., Reiber, J.H.C., Valstar, E.R., 2010. Detecting femur-insert collisions to improve precision of fluoroscopic knee arthroplasty analysis. J. Biomech. 43, 694-700.

Rehana, K., Tabish, S.A., Gojwari, T., Ahmad, R., Abdul, H., 2013. Unit cost of CT scan and MRI at a large tertiary care teaching hospital in North India. Health (N. Y.) 5, 2059-2063.

Röstlund, T., Carlsson, L., Albrektsson, B., Albrektsson, T., 1989. Morphometrical studies of human femoral condyles. J. Biomed. Eng. 11, 442-448.

Simileysky, A., Ridenour, D., Hull, M.L., 2021. Circle-based model to estimate error in using the lowest points to indicate locations of contact developed by the femoral condyles on the tibial insert in total knee arthroplasty. J. Biomech. 120, 110365.

Tanifuji, O., Sato, T., Kobayashi, K., Mochizuki, T., Koga, Y., Yamagiwa, H., Omori, G., Endo, N., 2011. Three-dimensional in vivo motion analysis of normal knees using single-plane fluoroscopy. J. Orthop. Sci. 16, 710-718.

Walker, P.S., Heller, Y., Yildirim, G., Immerman, I., 2011. Reference axes for comparing the motion of knee replacements with the anatomic knee. Knee 18, 312-316.

White, D., Chelule, K.L., Seedhom, B.B., 2008. Accuracy of MRI vs CT imaging with particular reference to patient specific templates for total knee replacement surgery. Int. J. Med. Robot. 4, 224-231.

Yin, L., Chen, K., Guo, L., Cheng, L., Wang, F., Yang, L., 2015. Identifying the functional flexion-extension axis of the knee: An in-vivo kinematics study. PLoS One 10, e0128877.

You, B.M., Siy, P., Anderst, W., Tashman, S., 2001. In vivo measurement of 3-D skeletal kinematics from sequences of biplane radiographs: Application to knee kinematics. IEEE Trans. Med. Imaging 20, 514-525.

FIGURES/TABLES

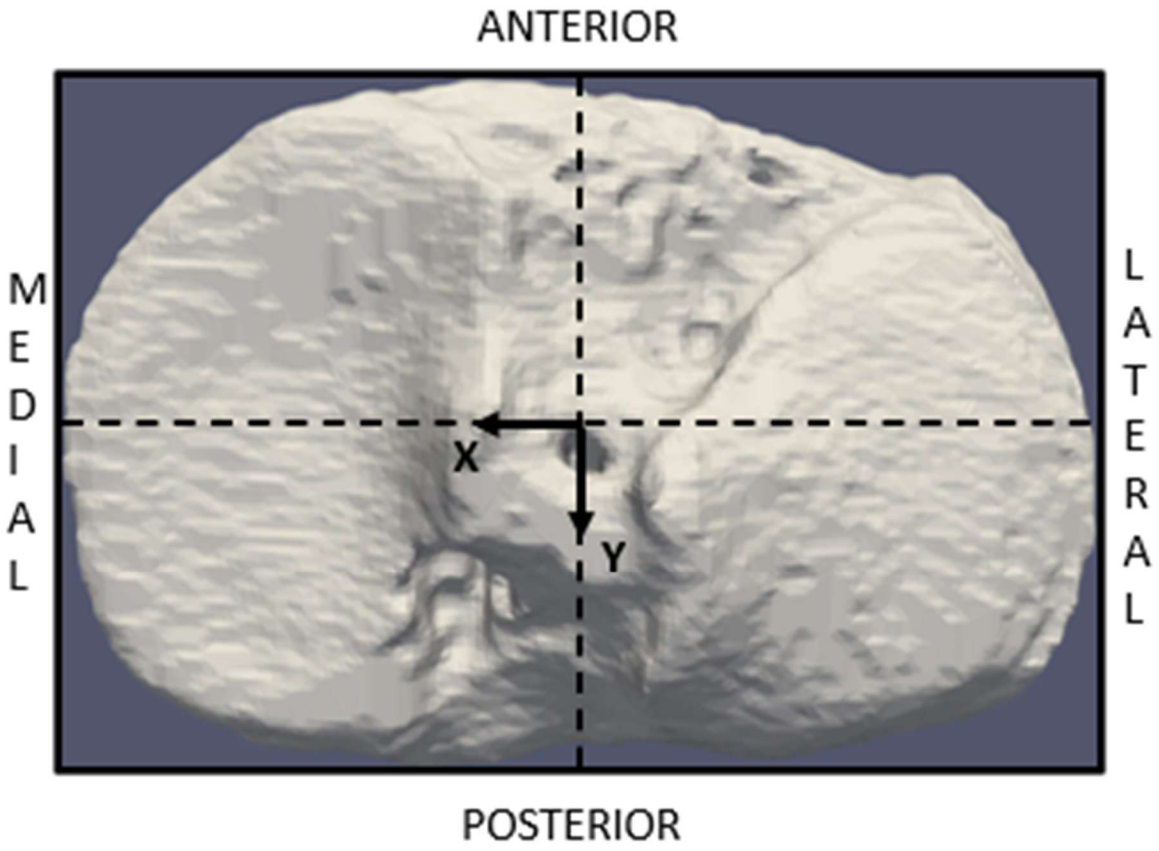

Figure 2.1. Axial view of the right proximal tibial plateau showing the tibial coordinate system used to report the AP femoral condyle positions in the medial and lateral compartments. The bounding box around the tibial plateau defined the directions of the AP and medial-lateral (ML) axes, and the center of the bounding box defined the origin of the coordinate system.

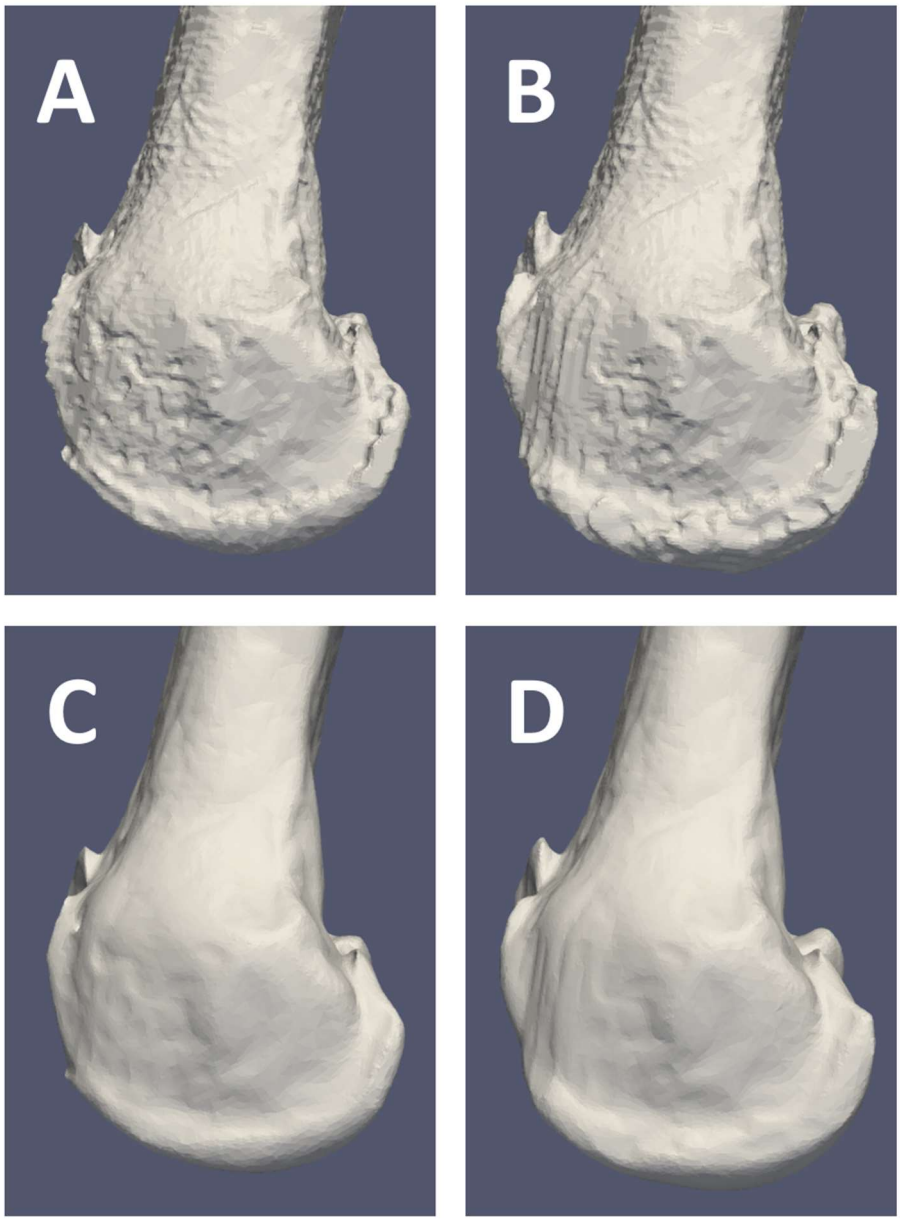

Figure 2.2. The four different MR model types used to determine the AP femoral condyle positions in the medial and lateral compartments. (A) The first type was a non-smoothed 3D bone model of the femur with no articular cartilage. (B) The second type was a non-smoothed 3D bone model of the femur with articular cartilage. (C) The third type was a smoothed 3D bone model of the femur with no articular cartilage. (D) The fourth type was a smoothed 3D bone model of the femur with articular cartilage.

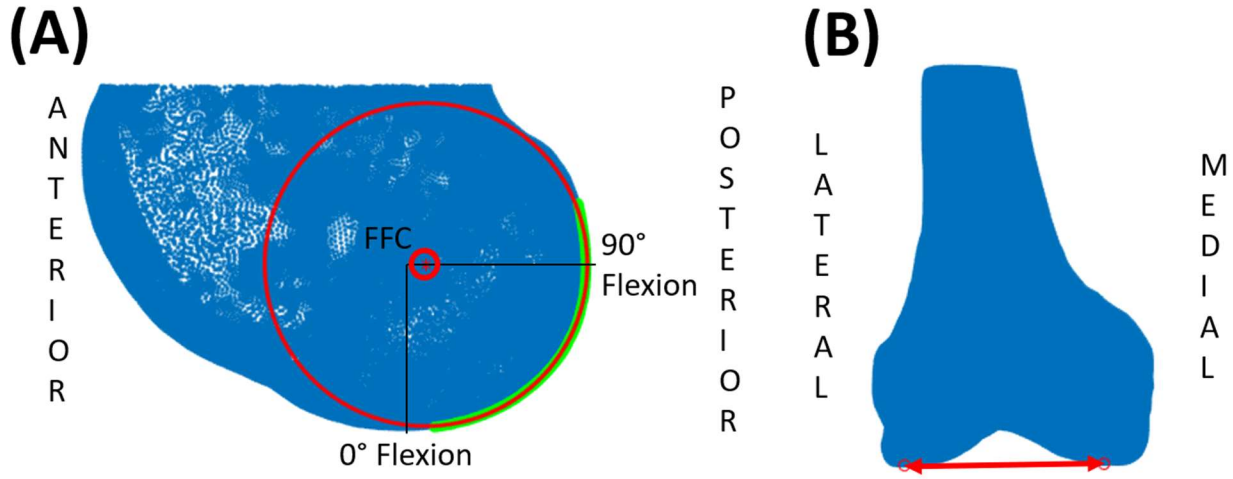

Figure 2.3. The process for the identifying the FFC on a femoral condyle. (A) Sagittal projection with the posterior medial and lateral femoral condyles superimposed. The 0° flexion point was defined by the most distal point on the femoral condyle with the femoral mechanical axis being vertical and parallel to the tibial mechanical axis in the sagittal view, and the 90° flexion point was defined by the most posterior point on the femoral condyle. A circle (red) was best fit to the outline of the posterior condyle's sagittal projection for flexion angles ranging from 10° to 110° (green). The center of the best-fit circle defined the AP and proximal-distal positions of the FFC. (B) Frontal projection of the right femur at full extension, which was perpendicular to the sagittal projection and parallel to the femoral mechanical axis. The ML position of each FFC was half the distance between the most distal points on each condyle. For the medial FFC, the sign of the ML position was positive for right femur and negative for the left femur (and vice versa for the lateral FFC).

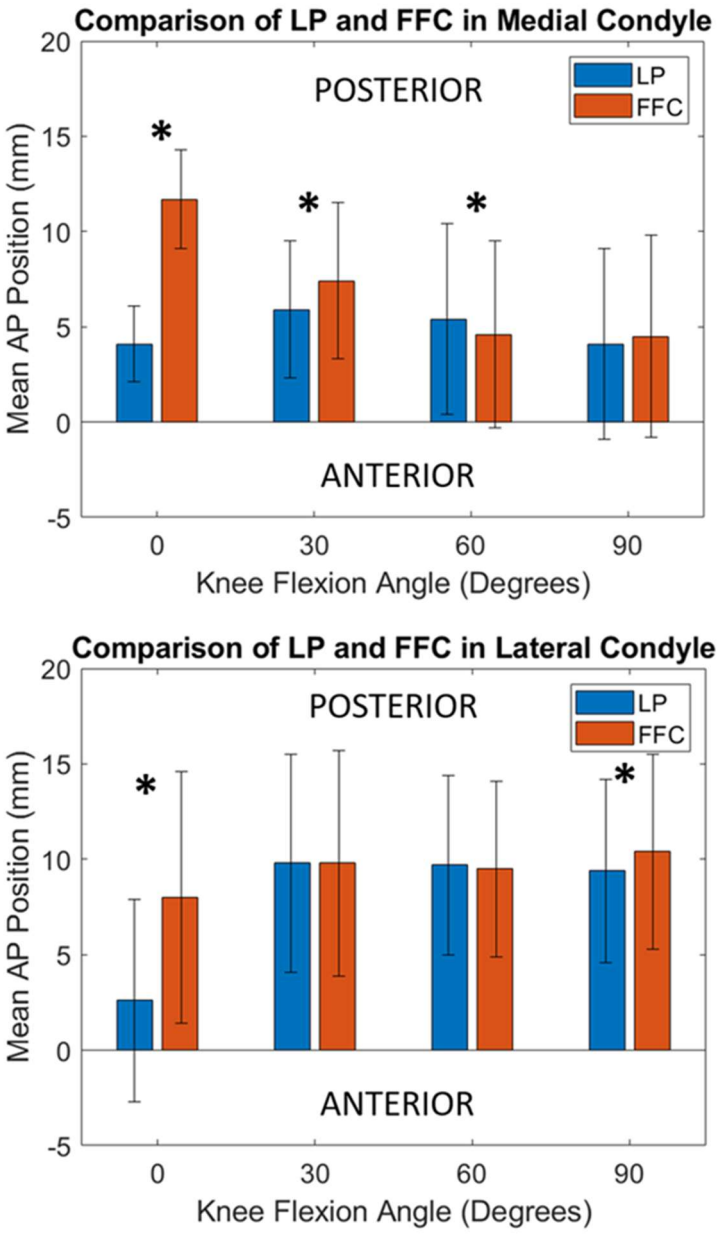

Figure 2.4. Bar graphs showing the mean AP positions of the LPs and FFCs in the medial and lateral compartments for the smooth 3D femur bone model with cartilage during a deep knee bend. The asterisks indicate statistically significant differences ($p < 0.05$). Error bars are ± 1 standard deviation.

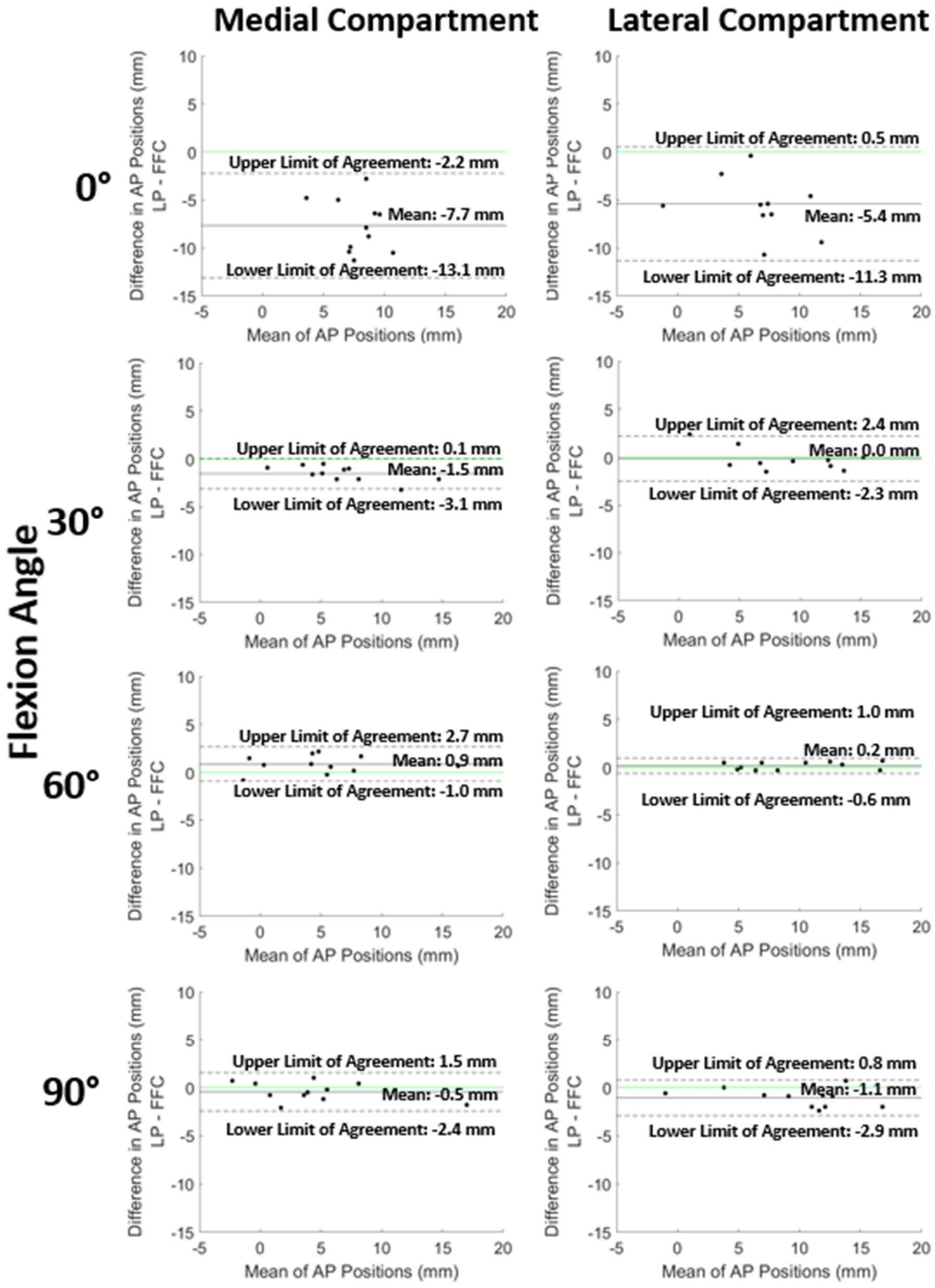

Figure 2.5. Bland-Altman plots showing differences in AP positions between the LPs and FFCs and limits of agreement at each flexion angle.

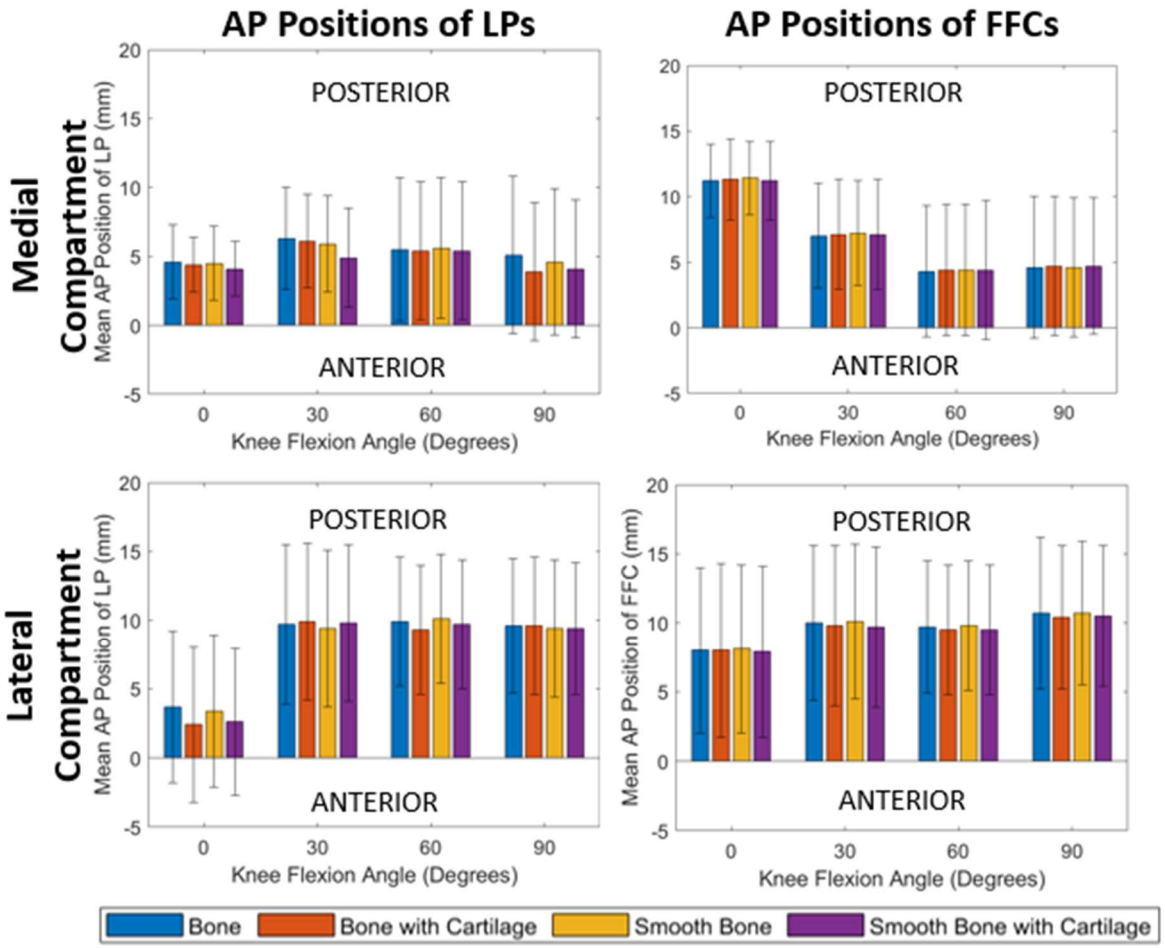

Figure 2.6. Bar graphs showing the mean AP positions of the LPs and FFCs in the medial and lateral compartments for four model types during a deep knee bend. Error bars are ± 1 standard deviation.

Chapter 3: Can a Planar Model More Accurately Determine Locations of Contact Developed by the Femoral Condyles on the Tibial Insert in Total Knee Arthroplasty than the Penetration Method?

ABSTRACT

Background: Knowledge of the anterior-posterior (AP) tibial contact locations are useful in assessing wear of tibial inserts and detecting posterior rim loading. The objectives of this study were to 1) create a new planar model that can determine AP tibial contact locations, 2) use the planar model to determine AP tibial contact locations for cadaveric TKA knees, and 3) determine whether errors of the planar model are lower than those of the penetration method.

Methods: A slopes-of-sagittal profiles (SSP) model was created using mathematical functions to simulate articular surfaces of the tibial insert and femoral condyles. AP tibial contact locations were calculated using the model and the penetration method and simultaneously measured with a tibial force sensor in 10 cadaveric TKA knees for four flexion angles (0°, 30°, 60°, and 90°) in each compartment during passive motion. For each method, the overall bias, overall precision, and overall root mean square error (RMSE) were calculated from the differences between the computed AP tibial contact locations and the measured locations.

Results: The SSP model had an overall bias of 0.6 mm and precision of 2.8 mm which were significantly greater than the overall bias of -0.1 mm ($p = 0.0369$) and overall precision of 2.0 mm ($p = 0.0021$) of the penetration method.

Conclusion: A planar model based on the analysis of single-plane radiographic images did not increase accuracy in AP tibial contact locations. Hence, the penetration method is preferred to determine AP tibial contact locations using single-plane radiography.

INTRODUCTION

Total knee arthroplasty (TKA) is a common treatment for tibiofemoral and patellofemoral osteoarthritis, with over 1 million procedures performed annually in the US alone (Kurtz et al., 2014). However, approximately one in five patients are dissatisfied with their outcome (Noble et al., 2006; Baker et al., 2007; Bourne et al., 2010). Two common contributors to patient dissatisfaction are wear of the polyethylene tibial insert and posterior rim loading of the tibial insert. Polyethylene insert wear has been associated with periprosthetic inflammation and implant loosening (Lewis, 1997; Naudie et al., 2007; Wilhelm et al., 2018) and is a common cause of TKA failure (Kim et al., 2014). Similarly, posterior rim loading has been associated with accelerated insert wear (Harman et al., 2001) and increased risk of TKA failure (Hamai et al., 2008). To reduce insert wear and incidence of posterior rim loading, developments in TKA have been made in the form of new surgical techniques, component alignment goals, and improved component designs. However, objective methods are needed to assess the efficacy of the developments.

To assess wear of the polyethylene tibial insert and detect posterior rim loading of tibial inserts with concave articular surfaces during activities of daily living, knowledge of the anterior-posterior (AP) tibial contact locations is useful. AP tibial contact locations are the locations of contact developed by the femoral component on the articular surface of the insert in the AP direction. Movements of the AP tibial contact locations during activities involving knee flexion are important to the analysis of tibial insert wear (Harman et al., 2001; Barnett et al., 2001; Bergmann et al., 2014; Wang et al., 2019) and extreme posterior movement particularly in the lateral tibial compartment identifies the occurrence of posterior rim loading (Howell et al., 2013; Nicolet-Petersen et al., 2019).

As a stepping stone to determining the AP tibial contact locations, the 3D spatial relationship between the femoral condyles and the tibial insert must be known. This relationship can be determined based on analysis of radiographs obtained from either single-plane (Banks & Hodge, 1996; Mahfouz et

al., 2003; Hoff et al., 1998) or dual-plane radiographs (Li et al., 2008) using 3D model to 2D image registration techniques. The errors in the six degrees of freedom (i.e. three translations and three rotations) are comparable except for the out-of-plane medial-lateral direction with single plane radiography (Prins et al., 2010). Since single-plane radiographic systems (e.g. fluoroscopes) are more widely available than specialized dual-plane systems, a method to accurately determine AP tibial contact locations using single-plane radiography would be beneficial.

One method that has been evaluated for accuracy using single-plane radiography is the penetration method. The penetration method calculates the tibial contact location as the centroid of the area of penetration of the insert of the tibial component by the femoral component (Li et al., 2006; Ross et al., 2017). If no penetration is present, then the contact location can be determined by finding the point on the femoral component with the shortest Euclidean distance between the tibial and femoral articular surfaces (Ross et al., 2017; Teeter et al., 2018). However, this method is prone to error when distance analysis is based on single-plane radiographs (Ross et al., 2017). Hence, there is a need for an improved method to determine the tibial contact location that is less susceptible to error using single-plane radiography.

Since the AP tibial contact location is determined by the AP movement of the femur with the respect to the tibia in conjunction with slopes of the articular surfaces (Simileysky et al., 2021), an approach for developing an improved method might be to develop a model based on these inputs. Hence, one objective of this study was to create a new planar model to determine AP tibial contact location for any femoral component design based on the slopes of the sagittal profiles of the articular surfaces of the femoral condyle and the tibial insert. A second objective was to use the new slopes-of-sagittal profiles (SSP) model to determine the AP tibial contact locations for cadaveric TKA knees during passive motion. A final objective was to determine whether errors of the planar model are lower than those of the penetration method.

METHODS

Model Description

As a starting point, a tibial component coordinate system was established (Figure 3.1). Using the tibial component coordinate system, two tibial insert coordinate systems were established: one for the medial compartment and one for the lateral compartment. For each tibial insert coordinate system, the origin was the dwell point (i.e. the deepest point) of the concave articular surface of the tibial insert in the respective compartment, and the orientation of the axes matched that of the tibial component coordinate system.

The SSP model (Figure 3.2) consists of two convex functions in the tibial insert coordinate system for each compartment, with one function representing the sagittal profile of the articular surface of the femoral condyle (function F(y)), and the other representing the concave sagittal cross-section of the articular surface of the tibial insert that passes through the dwell point (function P(y)). Anterior-posterior (AP) displacement (y_{AP}) occurs along the y-axis (+ posterior) and is defined as the distance along the y-axis between the lowest point of the femoral component and the dwell point of the tibial insert. The AP displacement is modeled by a shift in the femoral component function ($F(y\text{-}y_{AP})$). The tibial contact location is the point shared by the shifted femoral condyle function $F(y\text{-}y_{AP})$ and tibial insert function P(y), provided that $F(y\text{-}y_{AP})$ is elevated along the vertical z-axis (+ proximal) so that the functions intersect at one point.

A property of two convex functions that intersect at one point is that the slopes of the two functions will be the same at the intersection point. Taking the derivatives of the two functions yields:

$$\frac{d}{dy}[F(y - y_{AP})] = \frac{d}{dy}[P(y)] \qquad (1)$$

The AP tibial contact location is the value of y for which this equation is satisfied. Note that any vertical shift of $F(y\text{-}y_{AP})$ used to satisfy the single intersection point condition becomes irrelevant, since a shift of a function along the z-axis does not affect the slope of a function at any y-value.

The femoral condyle function F(y) was obtained by isolating the sagittal profile of the femoral condyle, dividing the profile into multiple segments of equal arc-length, and best fitting a circle to each of the segments. First, the sagittal view was defined by orienting the femoral component so that the medial and lateral lugs of the femoral component were superimposed (Figure 3.3). Next, the oriented component was rotated in the sagittal view so that the axis passing through the length of the lugs was proximal-distal. The femoral component was separated into medial and lateral halves, and the sagittal profile was obtained by isolating the outline of the articular surface for each condyle. The reference points for 0° flexion and 90° flexion were the most distal and most posterior points, respectively. These points were used to define the femoral condyle coordinate system (Figure 3.3). The 0° to 120° range of the sagittal profile was divided into nine segments. The segments were defined by center angles in 15° increments relative and included 7.5° of arc on either side of the center angle. A circle was best fit to each of the segments.

Similarly, the tibial insert function P(y) for each compartment was obtained by isolating the sagittal cross-section of the articular surface of the tibial insert that passes through the dwell point, dividing the cross-section into multiple segments of equal arc-length, and best fitting a circle to each of the segments. Using the tibial component coordinate system (Figure 3.1), the sagittal cross-section was obtained by isolating all points on the articular surface that were within 0.2 mm medially and laterally of a line parallel to the AP axis and passing through the dwell point. Additionally, a low-pass filter (Butterworth, 2^{nd} Order, cutoff frequency = 100 Hz) was applied forward and backward to the sagittal cross-section of the tibial insert to minimize noise while preserving the shape of the cross-section. Next, the reference point for 0° was the dwell point of the sagittal cross-section. Afterward, the -12° to 14° range of the sagittal cross-section relative to the 0° reference point was divided into fourteen segments. Segments were defined by center angles in 2° increments and included 2° of arc on either side of the center angle. A circle was best fit to each segment.

Data Collection

Unrestricted kinematically aligned TKA was performed on ten fresh-frozen cadaveric knee specimens using manual instruments (Howell et al., 2013), a transpatellar approach (Merican et al., 2009), and cruciate retaining femoral and tibial components (Persona, Zimmer Biomet, Warsaw, IN) implanted without ligament release. Once the cement mantles holding the components had cured, the tibial component was replaced by a custom tibial force sensor, which had 3D printed articular surfaces that matched the size and shape of the insert of the removed tibial component (Roth et al., 2017). The tibial force sensor measured the x and y coordinates of the center of pressure (i.e., tibial contact location) independently in each compartment and served as a gold standard from which errors in the SSP model and penetration method were determined. The precision of the sensor in measuring the AP tibial contact location was 1.5 mm.

Following the TKA procedure, each specimen was placed inverted into a testing fixture such that the tibia rested on top of the femur. The femur was rigidly fixed in all degrees of freedom except flexion-extension, while the tibia was constrained only in flexion-extension. This configuration allowed the knee to be positioned at any flexion angle between 0° and 120° (Ross et al., 2017). To ensure contact between the femoral component and tibial force sensor, an 89 N compressive load was applied to the distal end of the inverted tibia.

Four 24 cm x 30 cm single-plane radiographs were collected for each specimen, one for each flexion angle (0°, 30°, 60°, and 90°) with a neutral internal-external (IE) rotation of the tibia on the femur. The center of the X-ray source (model HF80H+, Min-Xray, Inc., Northbrook, IL) was aligned with the center of the film with a 1 m principal distance, and the specimen was placed in an oblique sagittal orientation of about 10° – 15° anterior between the X-ray source and film, about 25 cm from the film (Ross et al., 2017). Films were exposed to the X-ray source to produce radiographs (tube

voltage = 60 kV, tube current = 3.9 mA, exposure time = 0.28 s) while transducer signals generated by the sensor were simultaneously collected in each compartment.

Data Processing

The 3D position and orientation of the femoral component and tibial force sensor were determined using 3D model-to-2D image registration techniques (Banks & Hodge, 1996) and open-source software (https://sourceforge.net/projects/jointtrack/). 3D models of the components were projected onto the radiographs and adjusted in six degrees of freedom until the model silhouettes closely matched the component silhouettes in the radiographs. The femoral component was translated in the out-of-plane (i.e. medial-lateral) direction until it was centered over the tibial force sensor. This step was necessary because out-of-plane translation errors encountered with single-plane radiographs can result in the reconstruction of physiologically impossible poses (Fregly et al., 2005; Prins et al., 2010).

AP tibial contact locations in the tibial component coordinate system (Figure 3.1) were computed for each flexion angle using the SSP model and the penetration method. The first step in the SSP model was to find the AP locations of the lowest point on the sagittal profile of the femoral condyle and the dwell point on the insert of the tibial force sensor. The lowest point was the point on the femoral condyle that was closest to the plane defined by the distal surface of the tibial baseplate and the dwell point was the point on the articular surface of the insert of the tibial force sensor that was closest to the plane defined by the distal surface of the tibial baseplate. Next, the shifted femoral condyle function $F(y\text{-}y_{AP})$ and tibial insert function $P(y)$ were obtained following the procedure outlined in the model description. The AP tibial contact location was computed according to Equation l and the result was shifted by the AP magnitude of the dwell point so that the contact point was expressed in the tibial coordinate system.

The penetration method calculated the tibial contact location as the centroid of the area of penetration of the articular surface of the insert by the femoral component (Ross et al., 2017). The femoral component and tibial force sensor 3D models were imported into commercial software (Geomagic Control, 3D Systems, Cary, NC) in the same position and orientation at the flexion angles of interest. The penetration area was determined using Boolean logic to find the intersection of the two components in each compartment, and the AP tibial contact location was the geometric centroid of all points in the penetration area. If no penetration occurred, then the AP tibial contact location was the point on the femoral condyle that had the shortest Euclidean distance to the articular surface of the insert (Li et al., 2006).

For both the SSP model and the penetration method, mean AP tibial contact locations were reported for the four flexion angles (0°, 30°, 60°, and 90°) in each compartment. In calculating the mean, all AP tibial contact locations were standardized to the 53.3 mm AP dimension of the mid-sized tibial baseplate (Size F, Persona CR, Zimmer-Biomet) by multiplying each specimen's AP tibial contact location by the ratio of the AP dimension of the mid-sized baseplate to the AP dimension of their implanted baseplate.

Data Analysis

For the SSP model and the penetration method, the overall bias, overall precision, and overall root mean squared error (RMSE) were calculated from the errors in the AP tibial contact locations determined for four flexion angles (0°, 30°, 60°, and 90°) in both compartments (medial and lateral) of all ten specimens. The error in AP tibial contact location was the difference between the computed AP tibial contact location and the reference AP tibial contact location based on the tibial force sensor readings, with a positive error indicating that the computed contact point was more posterior than the reference contact point. The overall bias was the mean of the error in AP tibial contact location, the

overall precision was the pooled standard deviation of the error, and the overall RMSE was the root-mean-squared-sum of the overall bias and overall precision.

To determine whether the method significantly affected the overall mean error, a two-factor analysis of ANOVA with repeated measures was performed, where the two factors were the method type at two levels and flexion angle at four levels. Additionally, an F-test was performed to compare the precisions of the two methods. Significance was set at $p < 0.05$.

RESULTS

In the medial compartment, the mean AP tibial contact locations of the two methods differed by 0.7 mm or less over the four flexion angles. In the lateral compartment, the difference in the mean AP tibial contact locations was 1.6 mm or less (Figure 3.4B).

When evaluated against the tibial force sensor readings, the SSP model had an overall bias of 0.6 mm, an overall precision of 2.8 mm, and an overall RMSE of 2.8 mm. The penetration method had an overall bias of -0.1 mm, an overall precision of 2.0 mm, and an overall RMSE of 1.9 mm. The overall bias and precision of the SSP model were significantly greater than the penetration method ($p = 0.0369$ from two-factor ANOVA and $p = 0.0021$ from F-test, respectively).

DISCUSSION

The objectives of this study were to create a new planar model to determine the tibial contact location based on the lowest points and slopes of sagittal profiles of the articular surfaces, use the planar model to determine AP tibial contact locations for cadaveric TKA knees, and determine whether the errors of the planar model are lower than those of the penetration method. Based on the errors of the SSP model in comparison to those of the penetration method, the key finding was that the errors of the planar model were not lower.

To understand why the SSP model had larger errors, the SSP model's assumptions that affected the accuracy of the AP tibial contact location warrant critical review. One assumption was that the AP

movement of the lowest point and tibial contact location occurs along the sagittal cross-section of the tibial insert that passes through the dwell point. There are two circumstances which might violate this assumption. If IE rotation occurs, then the tibial contact locations will displace in the ML direction as well as in the AP direction. For this reason, the SSP model was applied strictly to knee specimens that were positioned with neutral IE rotation. Regardless, small amounts of IE rotation were still present within the knee specimens, as indicated by the lowest points in the lateral compartment moving more posterior during flexion than those in the medial compartment (Figure 3.4A).

The other circumstance occurs if the ML position of the lowest point does not lie in the sagittal cross-section passing through the dwell point in which case AP movement of the tibial contact location will occur along a different sagittal cross-section with a different profile shape. Hence, the computed AP tibial contact location would be affected. In this study, the femoral component was translated in the ML direction until it was centered over the tibial force sensor to mitigate out-of-plane translation errors with single-plane radiographs (Fregly et al., 2005; Prins et al., 2010). However, the true out-of-plane position of the femoral component relative to the tibial force sensor may be slightly off-center in the knee specimens, which would alter the ML position of the lowest point relative to the cross-section passing through the dwell point thus affecting the computed tibial contact location.

Another assumption was that multiple circles accurately describe the sagittal profiles and hence slopes of the articular surfaces of the tibial insert and femoral condyles. Since the SSP model relies on the derivatives of the sagittal profile functions F(y) and P(y) to accurately calculate the AP tibial contact location, the functions F(y) and P(y) not only must be a good fit for their respective profiles, but also they must accurately reflect the slopes of the articular surfaces. Each circular fit was assessed by calculating the relative root mean squared (RMS) radial deviation, which was found by normalizing the RMS radial deviation to the radius of the best-fit circle. For the tibial insert profile, all fourteen 4° arc segments were well approximated by circles (relative RMS radial deviation < 0.01%). For the

femoral profile, the seven 15° arc segments in the 0° - 90° range were well approximated by circles (relative RMS radial deviation < 0.10%) whereas the remaining two segments in the 90° - 120° range had greater deviation (relative RMS radial deviation between 0.29% and 0.92%). This larger deviation was likely due to the sharp decrease in the radius of curvature past 90° flexion of the femoral condyle profile (Figure 3.3). However poorer quality circle fits to arc segments past 90º would not have impacted our results since the flexion angle was limited to 90º.

Since 2D planar models are subject to somewhat increased error, our results suggest that a 3D surface model might be a fruitful approach since the assumptions above would be relaxed. A 3D surface model would consist of two surface functions, one representing the articular surface of the femoral condyle and the other representing the articular surface of the tibial insert. Since accurate ML and AP positions of each femoral condyle would be needed as inputs and since single-plane fluoroscopy is subject to large error in the ML position (Prins et al., 2010), dual-plane radiography would be needed to implement the 3D surface model. Although the authors are unable to pursue the development and error evaluation of a 3D surface model because of lack of access to a dual-plane radiography system, an important contribution of this paper is a new concept and demonstration of its implementation for developing such a model.

CONCLUSION

This study developed a new planar SSP model for computing the AP tibial contact locations, applied the model to cadaveric knee specimens, and showed that the planar model did not decrease the error compared to the penetration method. Hence, the penetration method remains the preferred method when calculating AP tibial contact locations using single-plane radiography.

ACKNOWLEDGMENT

The authors are grateful to Medacta USA, Inc. for financial support.

APPENDIX

The appendix elaborates on how a 3D surface model for finding tibial contact locations would be created. The surface model would use the same tibial insert coordinate system that the SSP model used and consist of two surface functions, with one function representing the articular surface of the femoral condyle (function F(x,y)), and the other representing the articular surface of the tibial insert (function P(x,y)). ML and AP displacements (x_{ML} and y_{AP}) would occur along the x-axis (+ lateral) and y-axis (+ posterior), respectively, and would be defined as the distances along the respective axes between the lowest point of the femoral component and the dwell point of the tibial insert. These displacements would be modeled by shifts in the femoral component function ($F(x\text{-}x_{ML}, y\text{-}y_{AP})$). The ML and AP coordinates of the tibial contact location would be defined as the coordinates where the slopes of the femoral condyle and tibial insert surface functions are equal. Since the 3D surface model operates on a higher dimension than does the 2D SSP model, the slopes would now be represented by the gradient of the surface functions. Taking the gradients of the two functions yields:

$$\nabla F(x - x_{ML}, y - y_{AP}) = \nabla P(x, y) \text{ , where } \nabla = \begin{bmatrix} \frac{\partial}{\partial x} \\ \frac{\partial}{\partial y} \end{bmatrix} (2)$$

By introducing the ML displacement, the 3D surface model would relax the first assumption of the 2D SSP model, allowing internal-external axial rotation of the tibia on the femur and ML movement of the lowest point and tibial contact location to be considered. However, it is impossible to know the true ML position of the lowest point using single-plane radiography, given the large out-of-plane translation error (Fregly et al., 2005; Prins et al., 2010). Hence, dual-plane radiography would be needed to implement the 3D surface model. Additionally, the chosen surface equations F(x,y) and P(x,y) would need to accurately describe the articular surfaces of the femoral condyle and tibial insert, respectively, while also considering the 3D orientation of the femoral component with respect to the tibial baseplate throughout flexion.

REFERENCES

Baker, P.N., van der Meulen, J.H., Lewsey, J., Gregg, P.J., 2007. The role of pain and function in determining patient satisfaction after total knee replacement. Data from the national joint registry for England and Wales. J. Bone. Jt. Surg. - Ser. B. 89, 893-900.

Banks, S.A., Hodge, W.A., 1996. Accurate measurement of three-dimensional knee replacement kinematics using single-plane fluoroscopy. IEEE Trans. Biomed. Eng. 43, 638-649.

Barnett, P.I., Fisher, J., Auger, D.D., Stone, M.H., Ingham, E., 2001. Comparison of wear in a total knee replacement under different kinematic conditions. J. Mater. Sci. Mater. Med. 12, 1039-1042.

Bergmann, G., Bender, A., Graichen, F., Dymke, J., Rohlmann, A., Trepczynski, A., Heller, M.O., Kutzner, I., 2014. Standardized loads acting in knee implants. PLoS One 9, e86035.

Bourne, R.B., Chesworth, B.M., Davis, A.M., Mahomed, N.N., Charron, K.D.J., 2010. Patient satisfaction after total knee arthroplasty: Who is satisfied and who is not? Clin. Orthop. Relat. Res. 468, 57-63.

Fregly, B.J., Rahman, H.A., Banks, S.A., 2005. Theoretical accuracy of model-based shape matching for measuring natural knee kinematics with single-plane fluoroscopy. J. Biomech. Eng. 127, 692-699.

Hamai, S., Miura, H., Higaki, H., Matsuda, S., Shimoto, T., Sasaki, K., Yoshizumi, M., Okazaki, K., Tsukamoto, N., Iwamoto, Y., 2008. Kinematic analysis of kneeling in cruciate-retaining and posterior-stabilized total knee arthroplasties. J. Orthop. Res. 26, 435-442.

Harman, M.K., Banks, S.A., Hodge, W.A., 2001. Polyethylene damage and knee kinematics after total knee arthroplasty. Clin. Orthop. Relat. Res. 392, 383-393.

Hoff, W.A., Komistek, R.D., Dennis, D.A., Gabriel, S.M., Walker, S.A., 1998. Three-dimensional determination of femoral-tibial contact positions under in vivo conditions using fluoroscopy. Clin. Biomech. 13, 455-472.

Howell, S.M., Hodapp, E.E., Vernace, J.V., Hull, M.L., Meade, T.D., 2013. Are undesirable contact kinematics minimized after kinematically aligned total knee arthroplasty? An intersurgeon analysis of consecutive patients. Knee Surg. Sports Traumatol. Arthrosc. 21, 2281-2287.

Howell, S.M., Papadopoulos, S., Kuznik, K.T., Hull, M.L., 2013. Accurate alignment and high function after kinematically aligned TKA performed with generic instruments. Knee Surg. Sports Traumatol. Arthrosc. 21, 2271-2280.

Kim, K.T., Lee, S., Ko, D.O., Seo, B.S., Jung, W.S., Chang, B.K., 2014. Causes of failure after total knee arthroplasty in osteoarthritis patients 55 years of age or younger. Knee Surg. Relat. Res. 26, 13-19.

Kurtz, S.M., Ong, K.L., Lau, E., Bozic, K.J., 2014. Impact of the economic downturn on total joint replacement demand in the United States: Updated projections to 2021. J. Bone Joint Surg. Am. 96, 624-630.

Lewis, G., 1997. Polyethylene wear in total hip and knee arthroplasties. J. Biomed. Mater. Res. 38, 55-75.

Li, G., Suggs, J., Hanson, G., Durbhakula, S., Johnson, T., Freiberg, A., 2006. Three-dimensional tibiofemoral articular contact kinematics of a cruciate-retaining total knee arthroplasty. J. Bone. Jt. Surg. - Ser. A 88, 395-402.

Li, G., Van de Velde, S.K., Bingham, J.T., 2008. Validation of a non-invasive fluoroscopic imaging technique for the measurement of dynamic knee joint motion. J. Biomech. 41, 1616-1622.

Mahfouz, M.R., Hoff, W.A., Komistek, R.D., Dennis, D.A., 2003. A robust method for registration of three-dimensional knee implant models to two-dimensional fluoroscopy images. IEEE Trans. Med. Imaging 22, 1561-1574.

Merican, A.M., Ghosh, K.M., Deehan, D.J., Amis, A.A., 2009. The transpatellar approach for the knee in the laboratory. J. Orthop. Res. 27, 330-334.

Naudie, D.D.R., Ammeen, D.J., Engh, G.A., Rorabeck, C.H., 2007. Wear and osteolysis around total knee arthroplasty. J. Am. Acad. Orthop. Surg. 15, 53-64.

Nicolet-Petersen, S., Saiz, A., Shelton, T., Howell, S.M., Hull, M.L., 2020. Small differences in tibial contact locations following kinematically aligned TKA from the native contralateral knee. Knee Surg. Sports Traumatol. Arthrosc. 28, 2893-2904.

Noble, P.C., Conditt, M.A., Cook, K.F., Mathis, K.B., 2006. The John Insall Award: Patient expectations affect satisfaction with total knee arthroplasty. Clin. Orthop. Relat. Res. 452, 35-43.

Prins, A.H., Kaptein, B.L., Stoel, B.C., Reiber, J.H.C., Valstar, E.R., 2010. Detecting femur-insert collisions to improve precision of fluoroscopic knee arthroplasty analysis. J. Biomech. 43, 694-700.

Ross, D.S., Howell, S.M., Hull, M.L., 2017. Errors in calculating anterior-posterior tibial contact locations in total knee arthroplasty using three-dimensional model to two-dimensional image registration in radiographs: an in vitro study of two methods. J. Biomech. Eng. 139, 121003.

Roth, J.D., Howell, S.M., Hull, M.L., 2017. An improved tibial force sensor to compute contact forces and contact locations in vitro after total knee arthroplasty. J. Biomech. Eng. 139, 041001.

Simileysky, A., Ridenour, D., Hull, M.L., 2021. Circle-based model to estimate error in using the lowest points to indicate locations of contact developed by the femoral condyles on the tibial insert in total knee arthroplasty. J. Biomech. 120, 110365.

Teeter, M.G., Perry, K.I., Yuan, X., Howard, J.L., Lanting, B.A., 2018. Contact kinematics correlates to tibial component migration following single radius posterior stabilized knee replacement. J. Arthroplasty 33, 740-745.

Wang, X.H., Li, H., Dong, X., Zhao, F., Cheng, C.K., 2019. Comparison of ISO 14243-1 to ASTM F3141 in terms of wearing of knee prostheses. Clin. Biomech. 63, 34-40.

Wilhelm, S.K., Henrichsen, J.L., Siljander, M., Moore, D., Karadsheh, M., 2018. Polyethylene in total knee arthroplasty: Where are we now? J. Orthop. Surg. (Hong Kong) 26, 1-7.

FIGURES/TABLES

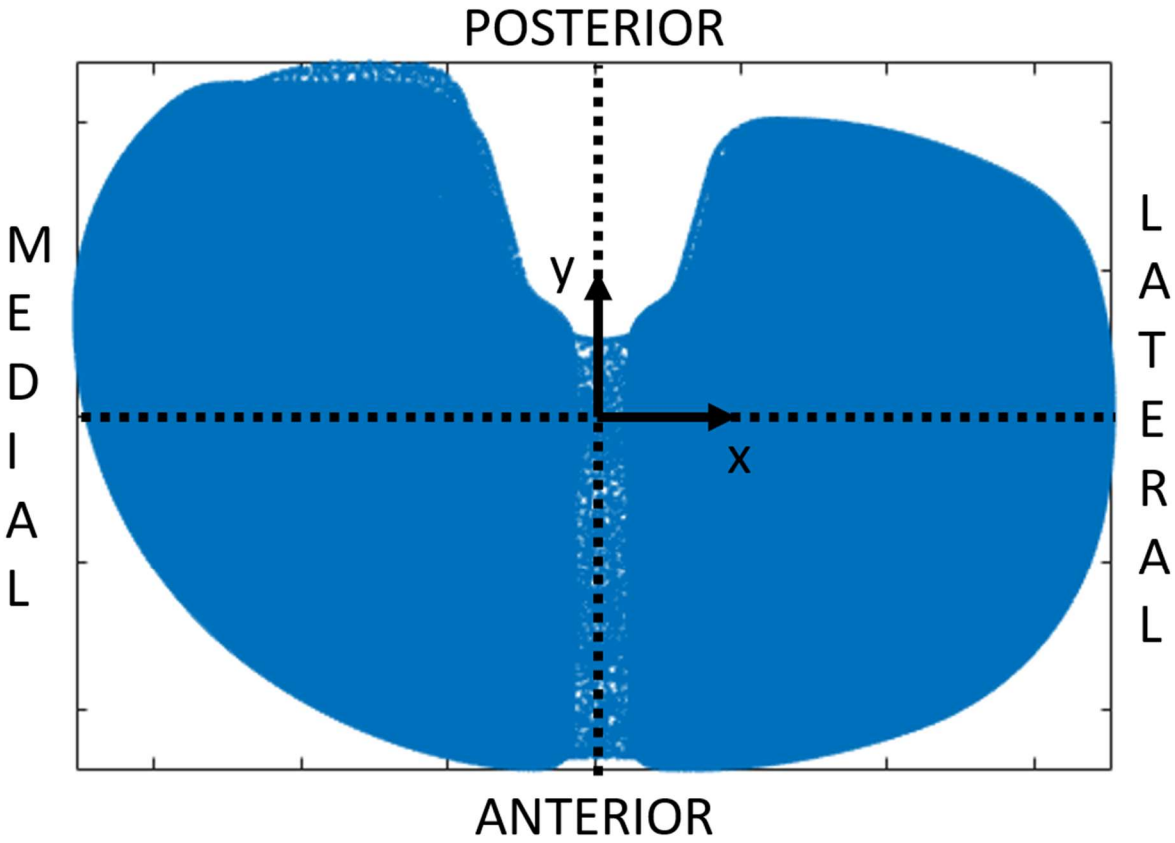

Figure 3.1. Axial view of tibial baseplate showing the tibial component coordinate system used to find the sagittal cross-section of the tibial insert that passes through the dwell point, and to report the AP tibial contact locations in the medial and lateral compartments. The bounding box around the tibial plateau defined the directions of the ML and AP axes (x and y axes, respectively), and the center of the bounding box defined the origin of the coordinate system.

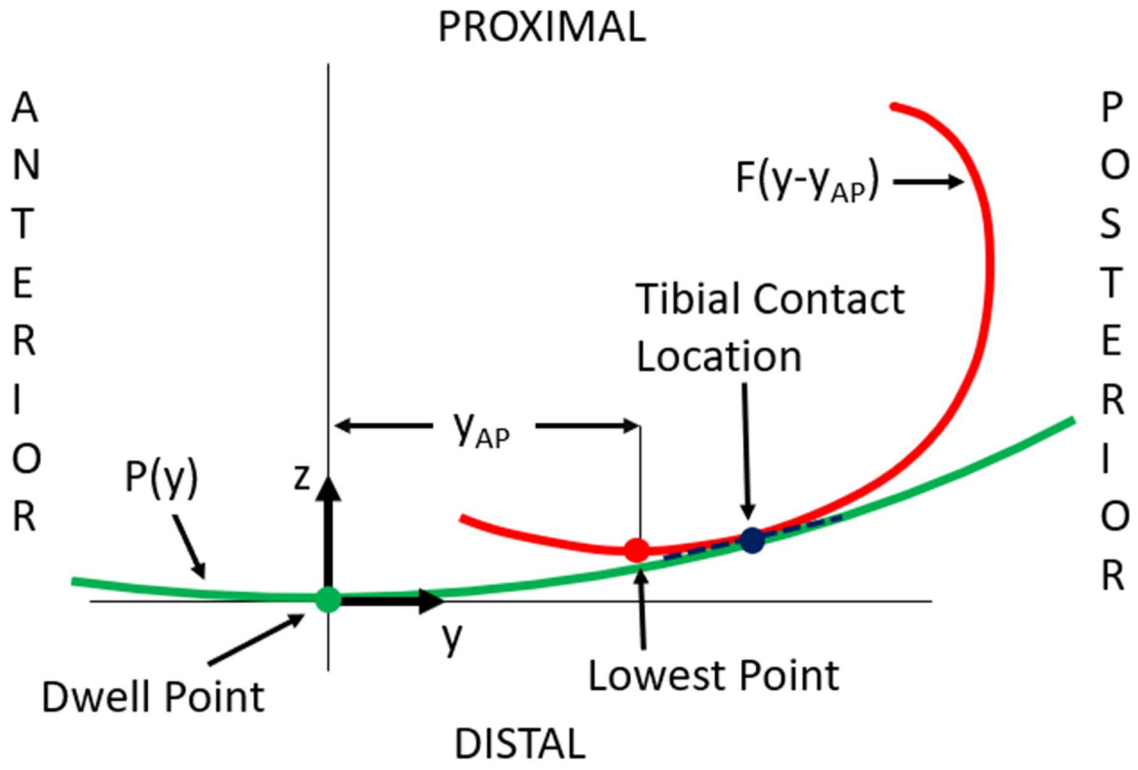

Figure 3.2. Illustration of the slopes-of-sagittal profiles (SSP) model in the tibial insert coordinate system, consisting of two convex functions representing the sagittal profile of the articular surface of the femoral component (red) and the concave sagittal cross-section of the articular surface of the tibial insert that passes through the dwell point (green). AP displacement (y_{AP}) is defined as the distance along the y-axis between the lowest point of the femoral condyle and the dwell point of the tibial insert. When y_{AP} is zero, the AP position of the lowest point coincides with the AP position of the dwell point. The tibial contact location (blue) is the point where the slopes of P(y) and F(y-y_{AP}) are equal (as indicated by the blue dashed line).

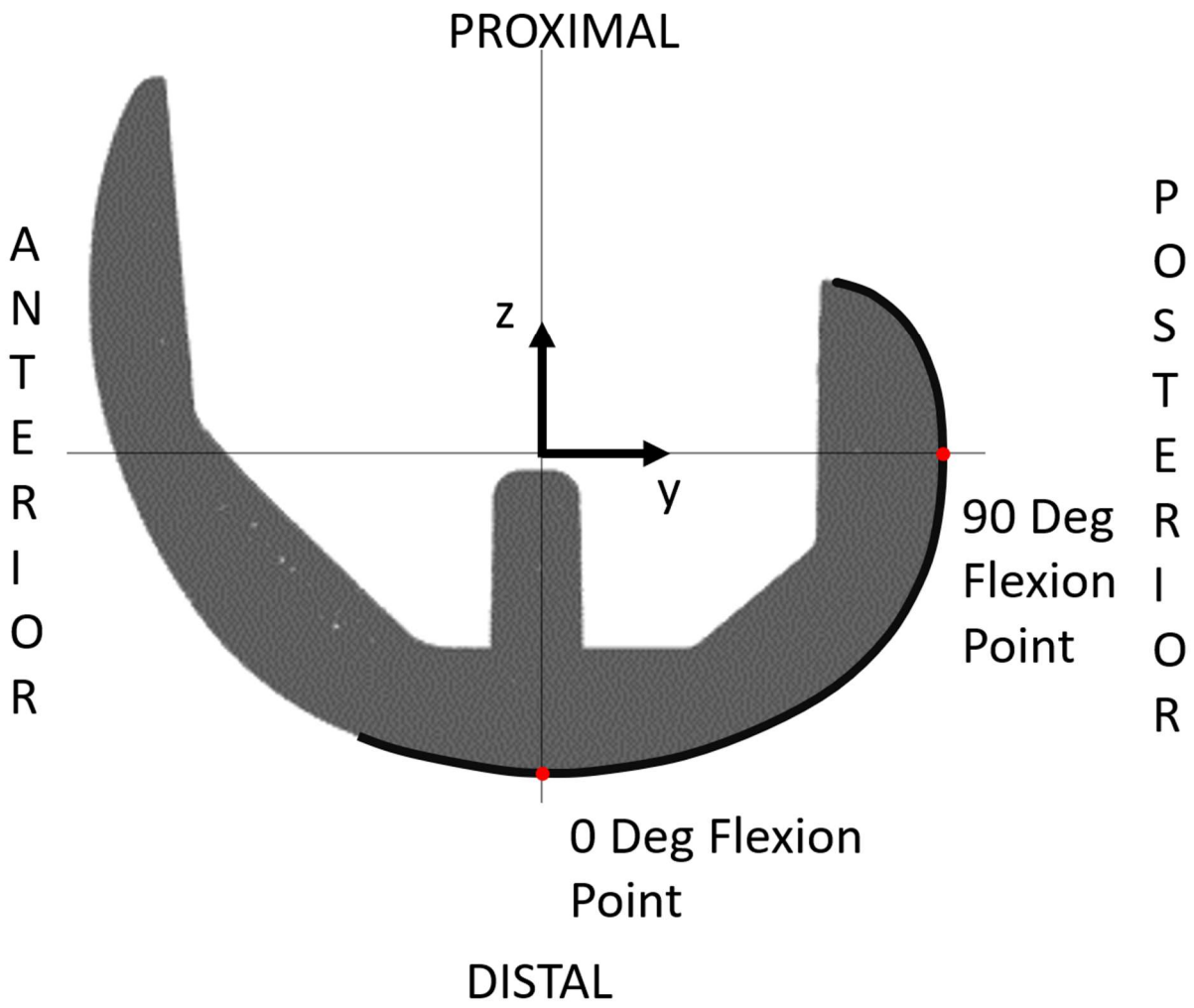

Figure 3.3. Sagittal view of the femoral component showing the femoral condyle coordinate system. The 0° flexion point was defined by the most distal point on the femoral condyle with the axis passing through the height of the lugs oriented proximal-distal in the sagittal view, and the 90° flexion point was defined by the most posterior point on the femoral condyle. The origin was the intersection of the proximal-distal line passing through the 0° flexion point and the anterior-posterior line passing through the 90° flexion point. The sagittal profile of the articular surface of the femoral condyle is outlined in black.

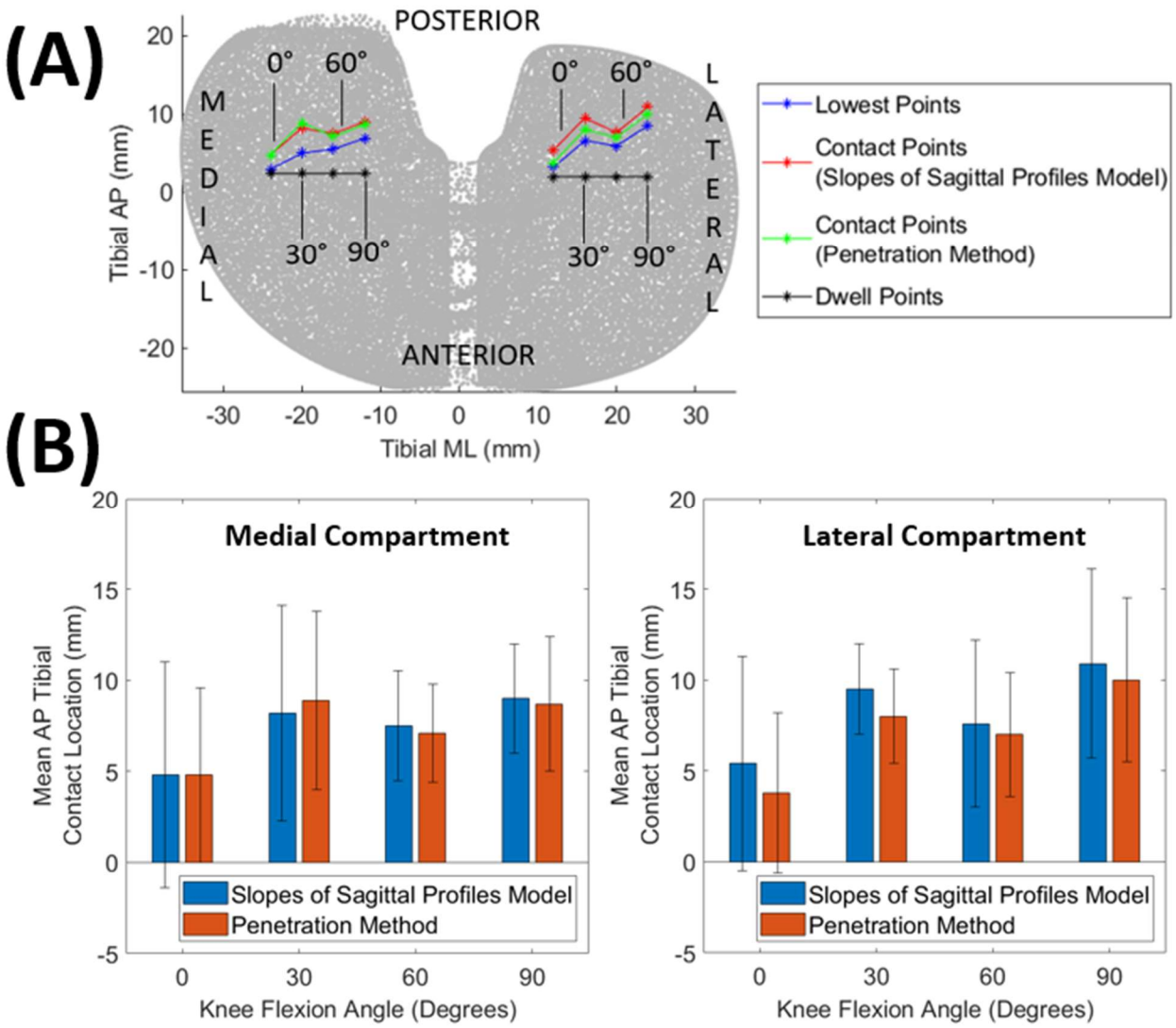

Figure 3.4. (A) Mean AP locations of the lowest points, dwell points, and tibial contact points for the SSP model and penetration method for four flexion angles in each compartment. (B) Plots of the mean and standard deviation of the AP tibial contact locations in the medial and lateral compartments for the SSP model and penetration method.